Geochimica et Cosmochimica Acta
Volume 82, 1 April 2012, Pages 92–112
http://dx.doi.org/10.1016/j.gca.2011.02.007

Mercury dynamics in lake sediments

Stéphane Feyte[a], Charles Gobeil[a,*], André Tessier[a], Daniel Cossa[b]

[a] INRS-ETE, Université du Québec, 490 de la Couronne, Québec, QC, Canada G1K 9A9
[b] Ifremer, Centre Méditerranée, BP330, 83507 La Seyne sur Mer, France

* : Corresponding author :
Tel.: +1 418 654 2589; fax: +1 418 654 2600.
E-mail address: Charles.Gobeil@ete.inrs.ca (C. Gobeil).

Abstract:

Triplicate porewater depth-profiles of pH and concentrations of total Hg (Hg_T), methylmercury (MeHg), Fe, Mn, sulfate, total sulfide, total zero-valent sulfur, organic C and major ions were determined at two sampling dates in a perennially oxygenated basin and a seasonally anoxic basin from Lake Tantaré, a Canadian Shield lake. The vertical distribution of Hg_T, MeHg, acid volatile sulfide, total S, Fe, Mn, Al and organic C were also determined in dated sediment cores from the same lake basins and from the deepest site of two other lakes, one also located in the Canadian Shield and the other in the Northeastern part of the Appalachian Mountains. Application of a one-dimensional transport-reaction equation to the dissolved Hg_T and MeHg profiles constrains the depth intervals (zones) where these species are produced or consumed in the sedimentary column and yields estimates of net reaction rates of Hg_T or MeHg in each of the zones as well as their fluxes at the sediment–water interface.

Dissolved Hg_T and MeHg diffused from the overlying water into the sediments, except for MeHg at one of the sampling dates in the perennially oxygenated basin. About 97% and 50% of the MeHg flux to the sediments is presently deposited with settling particles in the perennially oxygenated and seasonally anoxic basins, respectively. Removal of porewater Hg_T and MeHg occurred at all dates and sampling sites. Comparison of the consumption zones of porewater Hg_T and MeHg with the profiles of ancillary parameters, coupled with thermodynamic calculations, suggest that pure Hg mineral phases do not form in the sediments, that Hg_T and MeHg adsorption onto authigenic Fe oxyhydroxides occurs in minor proportions, and that the association of Hg_T and MeHg to Fe sulfide phases or sulfidized organic matter is possible. Assuming that the net consumption of MeHg in the porewaters was essentially due to demethylation, an apparent first-order rate constant for MeHg demethylation of 0.04–0.8 d^{-1} was estimated. Production of porewater MeHg occurred only in the perennially oxygenated basin, at sediment depths where SO_4 was consumed. Assuming that the net production of porewater MeHg was essentially due to methylation, an apparent first-order rate constant for Hg methylation ranging between 0.006 d^{-1} and 0.1 d^{-1} was calculated. These field-derived Hg methylation and MeHg demethylation rate constant values are within the range of those derived from Hg-spiked experiments. We also show that the post-depositional redistribution of total Hg during the early stages of sediment diagenesis is minor and that the solid-phase Hg_T record can be used to reconstruct the evolution of the anthropogenic Hg_T deposition.

Mercury dynamics in lake sediments

Stéphane Feyte[1], Charles Gobeil[1,*], André Tessier[1], Daniel Cossa[2]

[1]*INRS-ETE, Université du Québec, 490 de la Couronne, Québec, QC, Canada G1K 9A9*

[2]*Ifremer, Centre Méditerranée, BP330, 83507 La Seyne sur Mer, France*

* Corresponding author. Fax: +1 418 654 2600

E-mail address: Charles.Gobeil@ete.inrs.ca

ABSTRACT

Triplicate porewater depth-profiles of pH and concentrations of total Hg (Hg_T), methylmercury (MeHg), Fe, Mn, sulfate, total sulfide, total zero-valent sulfur, organic C and major ions were determined at two sampling dates in a perennially oxygenated basin and a seasonally anoxic basin from Lake Tantaré, a Canadian Shield lake. The vertical distribution of Hg_T, MeHg, acid volatile sulfide, total S, Fe, Mn, Al and organic C were also determined in dated sediment cores from the same lake basins and from the deepest site of two other lakes, one also located in the Canadian Shield and the other in the Northeastern part of the Appalachian Mountains. Application of a one-dimensional transport-reaction equation to the dissolved Hg_T and MeHg profiles constrains the depth intervals (zones) where these species are produced or consumed in the sedimentary column and yields estimates of net reaction rates of Hg_T or MeHg in each of the zones as well as their fluxes at the sediment water−interface.

Dissolved Hg_T and MeHg diffused from the overlying water into the sediments, except for MeHg at one of the sampling dates in the perennially oxygenated basin. About 97% and 50% of the MeHg flux to the sediments is presently deposited with settling particles in the perennially oxygenated and seasonally anoxic basins, respectively. Removal of porewater Hg_T and MeHg occurred at all dates and sampling sites. Comparison of the consumption zones of porewater Hg_T and MeHg with the profiles of ancillary parameters, coupled with thermodynamic calculations, suggest that pure Hg mineral phases do not form in the sediments, that Hg_T and MeHg adsorption onto authigenic Fe oxyhydroxides occurs in minor proportions, and that the association of Hg_T and MeHg to Fe sulfide phases or sulfidized organic matter is possible. Assuming that the net

consumption of MeHg in the porewaters was essentially due to demethylation, an apparent first-order rate constant for MeHg demethylation of 0.04-0.8 d^{-1} was estimated. Production of porewater MeHg occurred only in the perennially oxygenated basin, at sediment depths where SO_4 was consumed. Assuming that the net production of porewater MeHg was essentially due to methylation, an apparent first-order rate constant for Hg methylation ranging between 0.006 d^{-1} and 0.1 d^{-1} was calculated. These field-derived Hg methylation and MeHg demethylation rate constant values are within the range of those derived from Hg-spiked experiments. We also show that the post-depositional redistribution of total Hg during the early stages of sediment diagenesis is minor and that the solid-phase Hg_T record can be used to reconstruct the evolution of the anthropogenic Hg_T deposition.

1. INTRODUCTION

The increase in atmospheric deposition of mercury as a result of industrialization has stimulated the *in situ* production of methylmercury (MeHg) in aquatic systems and the incorporation of this neurotoxic compound into food chains (Evers et al., 1998; Hammerschmidt and Fitzgerald, 2006b; Munthe et al., 2007). The potential harmful consequences for human health and wildlife and possible adverse economical effects on the fishing industry raised by this issue have led to a marked interest over recent years for unraveling Hg cycling in aquatic systems (Fitzgerald et al., 2007). This study is in line with this general objective; it focuses on Hg dynamics in recent sediment deposits which are considered to be a key location for MeHg formation (Krabbenhoft et al., 1998; Kainz et al., 2003; Hammerschmidt et al., 2006).

Current inferences on *in situ* Hg_T and MeHg mobility and on the processes involving these species in modern sediments are mostly derived from measurements in the solid phase alone (Lockhart et al., 2000; Rydberg et al., 2008) or from laboratory experiments involving bacterial cultures (Compeau and Bartha, 1985) or incubations of Hg-spiked pure solid phases, sediments or lake water (Gunneriusson et al., 1995; Tiffreau et al., 1995; Miller, 2006; Ramlal et al., 1986; Hintelmann et al., 2000; Eckley et al., 2005). We submit that measuring Hg_T, MeHg and ancillary parameters in sediments and porewaters, combined with thermodynamic and kinetic modeling, provides an alternative to constrain *in situ* Hg_T and MeHg mobility, physico-chemical processes involving Hg_T and MeHg and their reaction kinetics. Although porewaters are sensitive indicators of reactions that occur in the solid phase, most studies reporting porewater profiles of Hg_T and MeHg, with a few exceptions (Goulet et al., 2007; Merritt and Amirbahman, 2007, 2008), only provided a qualitative interpretation of their results.

2. METHODS

In this paper, the concentrations of dissolved and solid-phase species X are designated by [X] and {X}, respectively. We assume that dissolved non-methylated Hg concentration ($[Hg_{NM}]$) is the difference between dissolved total Hg ($[Hg_T]$) and dissolved monomethylmercury ([MeHg]) concentrations.

2.1. Study areas

Three oligotrophic headwater lakes (Tantaré, Bédard and Holland) located in the Province of Québec (Eastern Canada) were investigated (Fig. 1). Their geographical coordinates, geological setting, altitude, water column pH, hypolimnetic oxygenation conditions as well as their surface

and watershed areas are given in Table 1. The only inputs of anthropogenic Hg into these lakes are from atmospheric deposition since their watersheds have never been inhabited; the watersheds have also not been affected by wildfire or lumbering, except that of Lake Bédard where tree cutting occurred several decades ago. Lakes Tantaré and Bédard are situated within 50 km of Québec City (~500,000 inhabitants), in a Provincial ecological reserve and in the protected Montmorency Forest, respectively. In Lake Tantaré, two adjacent basins separated by a shallow sill (~2 m) have been sampled: Basin A is 15 m deep and Basin B, which is upstream from Basin A (see Fig. 1), is 22 m deep. Both Basins A and B develop a thermal stratification which shifts from about 4 m depth at the end of May to 10 m depth at the end of October. The hypolimnion of Basin B, in contrast to that of Basin A, becomes anoxic ($[O_2]$ (< 0.01 mg L^{-1}) by mid-summer. Lake Holland is situated in the Gaspé Peninsula, 8 km from Murdochville, a small city (< 3,000 inhabitants) where a non-ferrous metal smelter (103,000 T of copper/zinc and 164,600 T of sulfuric acids produced in 1995; Newhook et al., 2003) operated from 1951 to 2002. Maximum depths in Lakes Bédard and Holland are 10 and 11 m, respectively.

2.2. Sampling

Sediment cores were collected by divers with 9.5-cm internal diameter butyrate tubes at the deepest site of each lake or basin between June 2003 and June 2006 (Table 1). The cores were extruded on shore and sectioned at 0.5-cm intervals from the sediment surface to 10 cm or 15 cm depth and then at 1-cm intervals to 30 cm depth. The sediment samples for subsequent acid volatile sulfide (AVS) measurements were individually sealed in plastic bags that were put into a larger

bag filled with anoxic sediment to prevent their oxidation, whereas those for all other measurements were kept in polyethylene containers.

Sheets of skived Teflon (7 × 15 cm) that had been inserted by divers across the sediment–water interface at the sampling site of Lake Tantaré Basin A in October 1993 were retrieved in August 2006, rinsed with lake water to remove living animals and sediment particles and stored in polyethylene containers. During the 13-yr deployment, authigenic Fe oxyhydroxides (Fe-ox) that are normally deposited onto sediment particles close to oxygenated sediment surface were collected by the Teflon sheets inserted in the sediments (Belzile et al., 1989). Fe-ox particles previously collected in this lake by the same technique were identified as poorly crystalline ferrihydrite and lepidocrocite by Fortin et al. (1993), using electron microscopy and X-ray diffraction. Authigenic Mn oxyhydroxides do not form in the sediments of this lake (see section 3.2) and thus, the material collected on Teflon sheets can be qualified as Fe-rich authigenic material.

Porewater samples were collected by *in situ* dialysis (Carignan et al., 1994) from 5 cm above the sediment−water interface to 10 cm below in the two basins of Lake Tantaré. The peepers used had two columns of 4-mL cells with a 1-cm vertical resolution. They were acid-washed and stored under nitrogen for at least two weeks. The cells were then filled with ultrapure water (> 18 MΩ cm) and covered with a pre-cleaned 0.2 µm nominal pore size polysulfone membrane (HT-200, Gelman). The assembled peepers were kept again under nitrogen for about two weeks, until their deployment. Twelve peepers were deployed by divers within an area of about 25 m^2 around the coring site in September 2005 and September 2006 in Basin A, which remains perennially oxic

138 ($[O_2] > 4$ mg L^{-1}), and in September 2006 and July 2007 in Basin B, when the bottom water was
139 anoxic ($[O_2] < 0.01$ mg L^{-1}) and oxic ($[O_2] > 4$ mg L^{-1}), respectively. Three peepers were sampled
140 to obtain triplicate measurements of pH and concentrations of dissolved organic carbon ([DOC]),
141 total sulfide ($\sum S(-II)$), total zero-valent sulfur ($\sum S(0)$) and major anions. Water from the remaining
142 nine peepers was collected as follow in order to get three 24-mL samples for each sampling depth
143 for subsequent measurements of Hg_T, MeHg and major cations (Al, Ca, Fe, K, Mg, Mn and Na).
144 Water in the cells positioned at a given height above or below the sediment−water interface was
145 collected from three peepers by piercing the polysulfone membrane with an acid-cleaned plastic tip
146 fitted to a Gilson pipette and was pooled in previously acid-washed Teflon (PFA) bottles. After
147 shaking, a 1-mL aliquot was removed and transferred to a pre-acidified (10 µL of 2N ultra clean
148 HNO_3) vial for the measurements of the cations. The remaining 23-mL sample was acidified by
149 adding 115 µL of ultra clean concentrated HCl to the Teflon bottle, which was then sealed in
150 double plastic bags. To obtain sampling procedural blanks for $[Hg_T]$, [MeHg], $\sum S(-II)$, $\sum S(0)$ and
151 DOC, ultrapure water was processed at the sampling site similarly to the porewater samples.
152
153 **2.3. Analyses**
154
155 The method used to measure $[Hg_T]$ was modified from Bloom and Fitzgerald (1988). It is
156 similar to standard method No. 1631 from US EPA (USEPA, 2002). Briefly, $[Hg_T]$ was
157 determined by cold vapor atomic fluorescence spectrometry (CVAFS; Tekran® model 2500),
158 using external calibration after successive addition of BrCl to release Hg(II) from organic ligands,
159 and $SnCl_2$, to reduce Hg(II) to elemental Hg (Hg(0)), which was concentrated by gold
160 amalgamation prior to CVAFS detection. Detection limit (DL), which was determined daily as 3.3

161 times the standard deviation (SD) of analytical procedural blanks, was between 0.5 and 2 pM for a
162 10-mL water sample. Precision, determined from replicate measurements (n = 6), was better than
163 5% at 20 pM and 15% at 1 pM. Analytical accuracy was checked every day with the reference
164 material ORMS-3 from the National Research Council of Canada (NRCC). Dissolved MeHg,
165 which is not degraded during long-term storage (at least 250 days; Parker and Bloom, 2005), was
166 measured within 2-4 weeks after sample collection. It was converted to volatile methylmercury
167 hydride, separated by purge and cryo-trapping gas chromatography, and detected as Hg(0) by
168 CVAFS (Tekran Model 2500). The hydride generation technique used was that proposed by
169 Stoichev et al. (2004) and optimized by Cossa et al. (2009). Daily DL varied between 0.05 pM and
170 0.2 pM. Precision, determined from replicate samples (n = 6), was 6% at a [MeHg] of 0.5 pM.
171 Accuracy was checked using the certified reference material ERM-AE70 from the Institute for
172 Reference Materials and Measurements (IRMM, European Commission).
173
174 Solid-phase Hg_T was determined on 50-mg freeze-dried sediment aliquots using a mercury
175 analyzer (Milestone DMA-80). This method, also known as the US EPA standard method No.
176 7473 (USEPA, 2007), includes a pyrolysis step that releases Hg, which is then concentrated by Au
177 amalgamation and detected by atomic absorption spectrometry (Cossa et al., 2002). Detection limit
178 (3.3 SD of blanks) was 30 pmol g^{-1}. Precision, determined from replicate measurements (n = 10) of
179 a sediment sample was better than 5%. Accuracy, determined with the reference sediment MESS-3
180 from NRCC, was better than 5%. Solid-phase MeHg was only determined for Lake Tantaré
181 sediments and two different analytical methods were used. The method of Leermakers et al. (2001)
182 adapted by Cossa et al. (2002) was used to analyze Basin A samples. MeHg was released from
183 about 200-mg aliquots of freeze-dried sediments with HNO_3 (4 N), extracted with CH_2Cl_2 and

transferred into 40 mL of ultrapure water. After evaporation of the organic solvent, MeHg in the water phase was ethylated and purged on a Tenax-packed column. Ethylmethylmercury was then isolated from other volatile compounds by gas chromatography and quantified by CVAFS. Detection limit (3.3 SD of blanks) was 0.1 pmol g^{-1} and analytical precision was better than 15%. MeHg analysis of the CRM 405 material from the International Atomic Energy Agency (IAEA) yielded a recovery of 91±8%. The method used to analyze Basin B samples was based on the separation of organomercurials by gas chromatography, followed by ionisation of analytes in argon plasma and Hg detection by mass spectrometry (Leermakers et al., 2005). Briefly, a known quantity of an internal standard ($Me^{202}Hg$) was added to an aliquot of freeze-dried sediment which was then leached with 4 mL of HNO_3 (6N). After centrifugation and decantation, the pH was adjusted to 4 by adding ammonia and a sodium acetate-acetic acid buffer. MeHg was then propylated by adding sodium tetrapropylborate and the Hg compound was extracted in isooctane. The analysis of propylated MeHg was performed by gas chromatography coupled to a quadrupole ICP-MS. Detection limit was around 1 pmol g^{-1}. Precision, determined from replicate measurements (n = 6) of the CRM 405 material from IAEA, was better than 10% and the recovery was evaluated to 102%.

Porewater Fe, Mn, Ca, K, Mg and Na concentrations were obtained by inductively coupled plasma optical emission spectroscopy (ICP-OES; VISTA AX CCD) using external calibration. Sulfate was measured by ion chromatography, dissolved inorganic C by gas chromatography, dissolved organic C with a Shimadzu carbon analyzer, ΣS(-II) by colorimetry within 48 h of sample collection and ΣS(0) by square-wave cathodic stripping voltammetry (Wang et al., 1998). It should be noted that ΣS(-II) and ΣS(0) are defined as (Wang and Tessier, 2009): $\Sigma S(-II) = [H_2S] + [HS^-] + \Sigma[H_xS_nS^{x-2}]$ and $\Sigma S(0) = [S(0)_{(aq)}] + \Sigma n[H_xS_nS^{x-2}]$, where x (0−2) and n (1−7) are the

numbers of H and zero-valent S atoms in the polysulfide species $H_xS_nS^{x-2}$, respectively, and $S(0)_{(aq)}$ is the free dissolved zero-valent sulfur.

The analytical protocols for the measurements of solid-phase Al, Fe, Mn, organic C (C_{org}), total S (S_T), AVS, ^{210}Pb, ^{214}Pb and ^{137}Cs are described by Chappaz et al. (2008). Briefly, C_{org} concentration was determined using a NCS Carbo Erba analyzer. Aliquots of sediments were totally digested with HNO_3, $HClO_4$ and HF and Fe, Mn, Al and S_T concentrations were determined by ICP-OES. AVS concentrations were determined by acidification of wet sediments with 6 N HCl, and the sulfide released was trapped in a NaOH solution and measured by colorimetry. For sediment dating, dried sediment aliquots were placed in sealed vials for at least 1 month to achieve secular equilibrium of ^{222}Rn and ^{214}Pb with ^{226}Ra, and the activities of ^{137}Cs, ^{210}Pb and ^{214}Pb were measured by gamma spectrometry (Chappaz et al., 2008). Unsupported ^{210}Pb activity was obtained by subtracting ^{214}Pb activity from that of ^{210}Pb. The ^{210}Pb models used to determine sediment mass accumulation rates (ω; mg cm^{-2} yr^{-1}) and sediment ages are given by Couture et al. (2008, 2010a).

Areas of the Teflon sheets containing the Fe-rich authigenic deposits were cut and dissolved in 50% HCl for 48 h at room temperature. The resulting solutions were filtered through 0.4-µm pore size Teflon membranes, diluted 10 times and analyzed for Fe by inductively coupled plasma optical emission spectroscopy (ICP-OES; VISTA AX CCD), for C and N with a Shimadzu C N analyzer and for Hg_T and MeHg as described above for dissolved Hg_T and MeHg.

2.4. Calculations of chemical speciation

The speciation of Hg in porewater and overlying water was predicted with the computer code Windermere Humic Aqueous Model (WHAM 6; Tipping, 2002) using as inputs the average measured pH values and concentrations of dissolved Hg_{NM}, MeHg, Al, Ca, Fe, K, Mg, Mn, Na, Cl, SO_4, CO_3, $\Sigma S(-II)$, $\Sigma S(0)$, and humic (HA) and fulvic (FA) acids. The concentrations of HA and FA were calculated from those of DOC, assuming that dissolved organic matter contains 50% of C (Buffle, 1988) and that all DOC is humic substances with a ratio [FA]:[HA] of 9:1 (Malcolm, 1985). We updated the thermodynamic database of WHAM 6 with the thermodynamic constants for the reactions of Hg and MeHg listed in Table 2, which required adding MeHg and dissolved zero-valent S ($S(0)_{aq}$) as new components. To be compatible with the code format, all reactions expressed in terms of solid rhombic sulfur ($S(\alpha)_{8(s)}$) in the literature were rewritten in terms of $S(0)_{aq}$ assuming that $1/8S(\alpha)_{8(s)} = S(0)_{aq}$; $K_S = 10^{-6.68}$ (Wang and Tessier, 2009). The constants for the formation of Hg-sulfide and Hg-polysulfide complexes were those provided by Jay et al. (2000), whereas those for the formation of Hg and MeHg complexes with HA and FA were recently updated by Tipping (2007). However, some of the constants should be taken with caution, especially those for the formation of Hg and MeHg complexes with sulfide, polysulfides, and humic and fulvic acids. For instance, it is noteworthy that the species $HgS_{(aq)}$ has never been detected experimentally. For the formation of the HgS_yOH^- and $Hg(S_y)_2^{2-}$ complexes given by Jay et al. (2000), the value of y, which could not be specified by the authors, was arbitrary assumed to be 5.

2.5. Modeling the porewater profiles of Hg_T and MeHg in Lake Tantaré

The porewater Hg_T or MeHg profiles result from transport processes and reactions that release Hg_T or MeHg to or remove them from the aqueous phase. Assuming steady-state and neglecting

advective fluxes due to sediment burial, compaction or groundwater flow (Gallon et al., 2004), the distribution of porewater Hg_T can be described by the following one-dimensional mass balance equation (Boudreau, 1997):

$$\left(\frac{\partial \phi [Hg_T]}{\partial t}\right)_x = \frac{\partial}{\partial x}\left(\phi D_S + D_B \frac{\partial [Hg_T]}{\partial x}\right) + \phi \alpha ([Hg_T]_{burrow} - [Hg_T]) + R_{net}^{Hg} = 0 \quad (1)$$

where x represents depth (cm; positive downward), t is time (s), ϕ is sediment porosity, D_S is the effective diffusion coefficient of Hg species in sediments ($cm^2\ s^{-1}$), D_B is the biodiffusion coefficient ($cm^2\ s^{-1}$), α is the bioirrigation coefficient (s^{-1}), $[Hg_T]_{burrow}$ is Hg_T concentration in the burrows of benthic animals (mol cm^{-3} of porewater), which is assumed to be identical to that in the water overlying the sediments, and R_{net}^{Hg} is the net reaction rate (mol cm^{-3} of whole sediment s^{-1}) of Hg_T released to ($R_{net}^{Hg} > 0$) or consumed from ($R_{net}^{Hg} < 0$) the aqueous phase. A similar equation can be written for the distribution of dissolved MeHg, where Hg_T is replaced by MeHg in Eq. (1); the term R_{net}^{MeHg} then represents the net rate of MeHg production to or removal from porewater.

We assumed that $D_S = \phi^2 D_W$ (Berner, 1980) where D_W is the tracer diffusion coefficient of the major Hg (or MeHg) species present in porewater. Considering that major dissolved Hg_T species are complexes with sulfide and polysulfides in porewaters of both Basins A and B (see section 3.1), we adopted a D_W value of 9.5×10^{-6} cm^{-2} s^{-1} at 25 °C, as proposed by Gill et al. (1999) for inorganic Hg complexes. With regard to MeHg, we used the D_W value provided by Hammerschmidt and Fitzgerald (2004) for MeHgSH (1.2×10^{-5} cm^{-2} s^{-1} at 25 °C), the main species of dissolved MeHg according to our calculations with WHAM 6. The chosen D_W values for Hg_T

and MeHg were then corrected for *in situ* temperature at our sampling sites (4°C) with the Stokes-Einstein equation (Boudreau, 1997).

For modeling Basin A porewater Hg_T and $MeHg$ profiles, the value of biodiffusion coefficient (2.2×10^{-9} cm^2 s^{-1}) provided by Gallon et al. (2004) was used in Eq. (1). This value was determined on the basis of an extensive inventory at the sampling site of the benthic fauna, which comprises mostly chironomids (Hare et al., 1994), and of biodiffusion coefficients for chironomids (Matisoff and Wang, 2000). The bioirrigation coefficient (α) for Basin A was assumed to decrease linearly from α^0 at the sediment surface to zero at 10 cm depth, because chironomids are generally not found below this sediment depth (Matisoff and Wang, 1998), and α^0 was derived from the following relationship provided by Boudreau (1984):

$$\alpha^0 = \frac{D_S r_1}{(r_2^2 - r_1^2)(r_a - r_1)} \quad (2)$$

where r_1 is the radius of a chironomid's tube (assumed to be 0.1 cm), r_2 is half the distance between adjacent tubes (1.5 cm), and r_a is equal to $r_2 / 2$. Given the seasonal development of anoxia in Basin B, we assumed that the biodiffusion (D_B) and bioirrigation (α) coefficients were negligible for this basin.

Equation 1 was solved numerically for R_{net}^{Hg} or R_{net}^{MeHg} using the code PROFILE (Berg et al., 1998). PROFILE first determines the minimum number of equally spaced depth intervals (or zones) with uniform values of R_{net}^{Hg} or R_{net}^{MeHg} needed to fit a measured Hg_T or $MeHg$ profile with parabola sections, based on the least-squares criterion. Using statistical F-testing, it then

293 determines if combining adjacent zones with close values of R_{net}^{Hg} or R_{net}^{MeHg} can be done without
294 reducing the quality of the fit. This procedure allows an objective selection, among all the possible
295 solutions, of the one that gives the simplest R_{net}^{Hg} or R_{net}^{MeHg} depth functions, which show as
296 piecewise constant functions.
297
298 **3. RESULTS**
299
300 **3.1. Porewater**
301
302 The concentrations of dissolved Hg_T varied between DL and 9 pM in Basin A and between DL
303 and 40 pM in Basin B (Fig. 2a-d). These concentrations are among the lowest values reported for
304 freshwater environments such as Lake St. Pierre (4-20 pM; Goulet et al., 2007), Lakes Philips and
305 St. George (40-100 pM; He et al., 2007) and Lakes Clearwater and McFarlane (10-100 pM with
306 some values up to 200 pM; Belzile et al., 2008). Porewater MeHg concentrations varied between
307 DL and 1.3 pM in Basin A and between DL and 10 pM in Basin B (Fig. 2e-h) and represented
308 <1% to 20% of [Hg_T] with a few extreme values up to 45%. These concentrations are also among
309 the lowest values reported for porewaters in freshwater environments such as a seepage lake (0.5-8
310 pM; Hines et al., 2004), Lake St-Pierre (<0.05-9 pM; Goulet et al., 2007) and Lakes Philips and St.
311 George (5-30 pM; He et al., 2007). The fact that the [Hg_T] and [MeHg] profiles are defined by
312 multiple data points suggests that they are not shaped by sampling and handling artifacts.
313
314 In Basin A, the [Fe] profiles (Fig. 2i, j) displayed sharp concentration gradients close to the
315 sediment–water interface due to the intense recycling of Fe-ox (Chappaz et al., 2008).

316 Furthermore, consistent with the occurrence of oxygenated bottom water, [SO_4^{2-}] (Fig. 2u, v) was
317 relatively high and [ΣS(−II)] (Fig. 2m-n) was below detection limit in the sediment overlying
318 water. Sulfate concentration decreased with depth below the sediment−water interface whereas
319 [ΣS(−II)] progressively increased below 2−6 cm depth in the sediments, depending on the
320 sampling date. The vertical profiles of [Hg_T] and [MeHg], in contrast to those of [Fe], [SO_4^{2-}] and
321 [ΣS(−II)], which displayed sharp variations, were almost featureless, except for two [MeHg]
322 profiles showing a notable MeHg increase at 5-10 cm depth in September 2005 and at 1-6 cm
323 depth in September 2006. The lack of correlation between the profiles of [Hg_T] and [MeHg] and
324 those of [Fe] suggests that they are not coupled in a simple manner. The few trend dissimilarities
325 observed among the profiles of [MeHg] as well as those of [SO_4^{2-}], [ΣS(−II)] and [ΣS(0)] (Fig. 2q-
326 r) indicate some sediment lateral heterogeneity at the scale of our porewater sampling area (~25
327 m^2).
328
329 The concentration gradients found for most solutes (Hg_T, MeHg, Fe, SO_4, ΣS(−II)) above the
330 sediment–water interface in Basin B suggest that a few cm thick nepheloid layer was present above
331 the sediment surface during both sampling periods and that solutes were transported by diffusion
332 across this layer. Even though some lateral heterogeneity was evident from the profiles of the
333 various solutes, the relatively higher [SO_4^{2-}] and lower ΣS(−II) in the sediment overlying water in
334 July 2007 (Fig. 2x, p) than in October 2006 (Fig. 2w, o) reflected a shift in bottom water redox
335 conditions. However, the profiles of [Fe] displayed only subtle differences in vertical trends, if
336 any, among the sampling dates (Fig. 3k-l). All the [Fe] profiles suggest a weak remobilization of
337 Fe in the sediments and a small upward diffusive Fe flux across the sediment–water interface.
338 Despite these differences in redox conditions, the trends in the [Hg_T] and [MeHg] profiles

remained quite similar, i.e., [Hg_T] and [MeHg] were higher in the overlying water than in porewater and progressively decreased downwards to 2-5 cm depth below the sediment–water interface. As in Basin A, the [Hg_T] and [MeHg] profiles showed no obvious correlation with those of [Fe]. On the contrary to what was observed in Basin A, where sulfate reduction occurred in porewater, the [SO_4^{2-}], ΣS(–II) and ΣS(0) profiles indicate that sulfate reduction took place above the sediment–water interface in this basin.

Thermodynamic calculations with the code WHAM 6 predict that dissolved Hg speciation was markedly different in Basins A and B (Fig. 3a-h). Since the measurements of Hg and MeHg and those of other physico-chemical parameters could not all be carried out in samples collected from the same peepers, we used average values of all the physico-chemical parameters in calculating Hg and MeHg speciation. Given the heterogeneity observed among replicate profiles of some key parameters (e.g., ∑S(-II), ∑S(0), Hg_{NM}, MeHg; Fig. 2a-h and m-t), there is some uncertainty in the predicted Hg_{NM} and MeHg speciation shown in Fig. 3a-h. In the overlying water of Basin A, where sulfide and zero-valent S concentrations were below detection limit, Hg_{NM} was predicted to be present mostly as complexes with humic substances (>99%), and MeHg as CH_3HgOH (~90%). At porewater ΣS(–II) above detection limit in this basin, however, calculations predicted that most of Hg_{NM} was rather in the form of HgS_{aq}, with only 2-3% bound to humic substances, and that MeHg likely existed mainly as CH_3HgSH. As for Basin B, thermodynamic predictions are that most of the Hg_{NM} was in the form of polysulfide complexes when ΣS(0) was above 0.2 μM, and as sulfide complexes when ΣS(0) was below 0.2 μM. Most of the MeHg was predicted to be in the form of $MeHgS^-$ (18±3%) and MeHgSH (80±3%). Hg_{NM} and MeHg complexes with humic substances appear to be negligible (<1% for both) in Basin B even if porewater DOC was about 2-fold higher

362 in Basin B than in Basin A (data not shown). It is noteworthy that similar conclusions about the
363 speciation of Hg_{NM} and MeHg in sediment porewater were reached by Goulet et al. (2007) and
364 Merritt and Amirbahman (2007, 2008).
365
366 **3.2. Solid-phase**
367
368 Solid-phase Fe concentration sharply decreased in the top 2-cm layer of Lake Tantaré Basin
369 A sediments (Fig. 4g) and then remained nearly constant downwards. This near surface Fe
370 enrichment results from the intense redox recycling of Fe in the sediments of this basin (Laforte et
371 al., 2005); it is consistent with the sharp porewater [Fe] gradients close to the sediment−water
372 interface (Fig. 2i, j). If we assume that the concentration of authigenic Fe-ox in the top 0.5-cm
373 sediment layer is the difference between the measured {Fe} concentration in this layer and the
374 constant background {Fe} value below 15 cm depth, then $\{Fe\text{-}ox\} = 1.55 \times 10^{-3}$ mol g^{-1} (Table 3).
375 Comparable surface sediment Fe enrichment is absent from Basin B and from the other two lakes
376 where the bottom waters become seasonally anoxic (Fig. 4h-j). In Lakes Bédard and Holland
377 sediments, maximum {Fe} were coincidental with AVS peaks that occurred at 3.75-5.25 cm depth
378 (Fig. 4q, r). Sediment and porewater Mn profiles (Figs. 4g-j and 2i-l) did not show any evidence of
379 redox recycling of this element, consistent with the anoxic condition (Lakes Bédard and Holland
380 and Basin B of Lake Tantaré) or with the slightly acidic condition of porewater (Basin A of Lake
381 Tantaré; Laforte et al., 2005).
382
383 Organic C concentrations in the sediments of the three study lakes ranged from ~16% and
384 ~35%; they varied with depth in Lake Holland, but remained nearly monotonic in the other lakes

(Fig. 4 k-n). The average (±SD) $\{C_{org}\}$:{N} molar ratios of the sediments, over the whole cores, were 16.7 ± 0.7, 16.6 ± 2.2, 16.3 ± 2.3 and 13.7 ± 1.2 for Basins A and B of Lake Tantaré and for Lakes Bédard and Holland, respectively. Such large $\{C_{org}\}$:{N} ratios are consistent with organic matter being mainly humic substances derived from the watershed rather than autochtonous organic matter (Feyte et al., 2010); indeed, these ratios are much larger than those (6.4 - 6.6) reported for phytoplankton or for settling particles in a productive lake (Redfield, 1934; Hamilton-Taylor et al., 1984), but close to those of soil humic substances (Buffle, 1988). The $\{C_{org}\}$:{N} ratio in the top 0.5-cm sediment layer of Basin A was 15.5, a value very close to that measured (15.3 ± 3.4) in the Fe-rich diagenetic material collected on Teflon sheets (Table 3). Organic matter in surface sediment and that associated to the diagenetic material can thus be assumed to have the same origin. The slightly lower $\{C_{org}\}$:{N} molar ratios in surface sediments and in the diagenetic material than the average (± SD) ratio for the whole core (16.7 ± 0.7) are consistent with the presence of small amounts of autochtonous labile organic matter present at the sediment surface. Notably, the $\{C_{org}\}$:{Fe} molar ratio of 2.6 ± 0.3 (Table 3) found in the Fe-rich material indicates that it contains substantial amounts of organic matter. The $\{C_{org}\}$:{Fe} molar ratio of the diagenetic material is, however, much smaller than that measured in the top 0.5-cm layer of sediments (13; Table 3), thus indicating that most of humic substances in the sediments was not bound to Fe-ox but was present as organic coating on other solids or as separate particles.

At each of the sampling sites where AVS was measured, maximum concentrations occurred at depths ranging from 3.25 to 8.75 cm (Fig. 4o, q, r). The $\{S_T\}$ and {AVS} profiles exhibited subsurface maxima at the same depth in Lakes Bédard and Holland sediments, but not in those of Lake Tantaré Basin A where the S_T peak was slightly deeper than the AVS peak. An important

aspect of these results is that AVS represents only a minor fraction of $\{S_T\}$ in Lakes Tantaré and Bédard sediments and a small fraction in Lake Holland sediments. For instance, the inventories of AVS over the total length of the cores are equivalent to 0.5%, 3% and 26% of those of S_T for Lakes Tantaré (Basin A), Bédard and Holland, respectively. Using a non-steady state one-dimensional reactive transport modeling approach, Couture et al. (2010b) concluded that the AVS concentrations in Basin A sediments are about one order of magnitude lower than what they should be considering the sulfate reduction rate. If, as their model indicates, pyrite does not form in these sediments due to slow kinetics and low porewater $\sum$S(-II), the high rate of SO_4 reduction and the low AVS inventory could then only be reconciled by inferring that most of the sulfide produced became associated to the organic matter. Substantial laboratory and field evidences exist for the incorporation of dissolved sulfide to humic substances (e.g., Canfield et al., 1998; Einsield et al., 2008).

The concentrations of Hg_T measured in the sediments of the three study lakes ranged between 0.6 and 3.0 nmol g^{-1} (Fig. 4a-d). These values are typical of those reported for other lake sediments from North-Eastern United States to Northern Canada and Alaska (e.g. Perry et al., 2005; Fitzgerald et al., 2005; Engstrom et al., 2007; Mills et al., 2009; Muir et al., 2009). While the ranges for $\{Hg_T\}$ in Lake Tantaré Basins A and B were similar, their profiles exhibited striking differences (Fig. 4a, b). In Basin A, $\{Hg_T\}$ increased progressively toward the sediment surface from an average ($\pm$ SD) background value of 1.07 $\pm$ 0.08 nmol g^{-1} below 15 cm to an uppermost value of 3.0 nmol g^{-1} at the sediment surface. The $\{Hg_T\}$:{Fe} molar ratio in the Fe-rich material ($1.3 \pm 0.3 \times 10^{-7}$) was much lower than in the top 0.5-cm sediment layer (1.9×10^{-6}) (Table 3). In Basin B, $\{Hg_T\}$ increased from a background value of 0.91 $\pm$ 0.06 nmol g^{-1} at the bottom of the

core to a sub-surface maximum of 2.8 nmol g^{-1} at a depth of 5.25 cm and then decreased progressively to 2.3 nmol g^{-1} at the sediment surface. The average (± SD) partition coefficient for Hg_T ($K_D^{Hg} = \{Hg_T\}/[Hg_T]$) in sediments of Basins A and B ($\log K_D^{Hg} = 5.7 \pm 0.2$) is slightly higher than those reported for other freshwater sediments ($\log K_D^{Hg} = 3.7\text{-}4.5$; He et al., 2007; Goulet et al, 2007; Belzile et al., 2008). It is noteworthy that the profiles of the $\{Hg_T\}$:{Al} molar ratio and those of $\{Hg_T\}$ exhibited very similar trends in the two basins of Lake Tantaré and of Lake Bédard, but not in Lake Holland (Fig. 4a-d). The $\{Hg_T\}$:{Al} ratio varied between $7.2 \pm 0.7 \times 10^{-7}$ and 22×10^{-7} (Basin A) or 29×10^{-7} (Basin B) in Lake Tantaré sediments and between $7.1 \pm 0.4 \times 10^{-7}$ and 11.8×10^{-7} in those of Lake Bédard. In Lake Holland, the $\{Hg_T\}$:{Al} ratio varied steeply with depth; it decreased from the sediment−water interface (17×10^{-7}) to 13 cm depth (5.6×10^{-7}), increased sharply below this horizon to reach a maximum at 21 cm depth (34×10^{-7}) and then decreased to 20×10^{-7} at the bottom of the core. Note that all the $\{Hg_T\}$:{Al} values, even the preindustrial ones at the bottom of the cores, are higher than the average $\{Hg_T\}$:{Al} molar ratio in the Upper Continental Crust (0.7×10^{-7}; Wedepohl, 1995) suggesting that even the preindustrial $\{Hg_T\}$ does not comprise only lithogenic Hg.

The concentrations of sediment MeHg in Basins A and B of Lake Tantaré varied from 3 to 75 pmol g^{-1}, representing 0.2 to 2.5% of $\{Hg_T\}$ and are typical of those reported for other lake sediments of the North American continent (e.g. Ethier et al., 2010; He et al., 2007; Hines et al., 2004). The solid-phase distribution of MeHg in Basin A contrasts with that in Basin B. Surface sediments are enriched in {MeHg} in Basin A, but not in Basin B. Surface sediment enrichments in MeHg were also observed in other lake sediments and were attributed to MeHg production and/or deposition at the sediment surface and subsequent demethylation with sediment burial

(Hines et al., 2004; He et al., 2007; Rydberg et al., 2008). In the Fe-rich deposits collected with the Teflon sheets in Basin A, the average (n = 7) {MeHg}:{Fe} molar ratio was $6.5 \pm 1.9 \times 10^{-10}$, a much lower value than that found in the top 0.5-cm sediment layer (4.9×10^{-8}; Table 3). The average (± SD) partition coefficient for MeHg (K_D^{MeHg} = {MeHg}/[MeHg]) in Basin A and B sediments ($\log K_D^{MeHg} = 4.7 \pm 0.4$) was slightly higher than those reported for other lake sediments ($\log K_D^{MeHg} = 0.5\text{-}4$; He et al., 2007; Goulet et al., 2007).

4. DISCUSSION

4.1. Modeling the [Hg_T] profiles

The modeled [Hg_T] profiles for the average (n = 3) porewater Hg_T distribution in each basin of Lake Tantaré and sampling date as well as the zones of Hg_T production or consumption are shown in Fig. 3i-l whereas the values of the net rate (R_{net}^{Hg}) in each zone, numbered downward from the sediment–water interface, are given in Table 4. For calculating the average [Hg_T], we assumed a value of 0.5 DL for all undetected concentrations. In Basin A, the modeled [Hg_T] profiles were in relatively good agreement ($r^2 = 0.76\text{-}0.82$) with the measured profiles. In September 2005, there was a 6-cm thick zone of slow net Hg consumption ($R_{net}^{Hg} = -0.7 \times 10^{-21}$ mol cm^{-3} s^{-1}) just below the sediment–water interface, above a zone of slow net Hg_T production ($R_{net}^{Hg} = 2.4 \times 10^{-21}$ mol cm^{-3} s^{-1}). In September 2006, PROFILE suggests the occurrence of a single zone of slow net Hg_T consumption ($R_{net}^{Hg} = -0.8 \times 10^{-21}$ mol cm^{-3} s^{-1}) between the sediment–water interface and 10 cm depth. In Basin B, the R_{net}^{Hg} values provided by PROFILE were larger than those found in Basin A

476 and the modelled and measured [Hg_T] profiles were in better agreement (r^2 = 0.95-0.96). At both
477 sampling periods, there was consistently a 4-6-cm thick zone of relatively fast net consumption of
478 dissolved Hg_T (R_{net}^{Hg} = -3.6 × 10^{-21} mol cm^{-3} s^{-1} to -14 × 10^{-21} mol cm^{-3} s^{-1}) above a zone of
479 relatively fast net Hg_T production (R_{net}^{Hg} = 1.7 × 10^{-21} mol cm^{-3} s^{-1} to 11 × 10^{-21} mol cm^{-3} s^{-1}). Note
480 that the R_{net}^{Hg} values for the release of Hg_T to Lake Tantaré porewater were 3-15 times lower than
481 those reported by Merritt and Amirbahman (2007) for the highly contaminated Penobscot River-
482 Estuary sediments (R_{net}^{Hg} = 37 × 10^{-21} mol cm^{-3} s^{-1} to 52 × 10^{-21} mol cm^{-3} s^{-1}). As for the net rates of
483 Hg_T removal from porewater, they were of similar magnitude to those of the Penobscot River-
484 Estuary (R_{net}^{Hg} = -7.5 × 10^{-21} mol cm^{-3} s^{-1} to -14 × 10^{-21} mol cm^{-3} s^{-1}) only in Basin B sediments.
485
486 Thus, Fig. 3i-l indicates consistently that Hg_T is removed in zone 1, located just below the
487 sediment–water interface; thickness of the zone (4 - 10 cm) and intensity of net Hg_T removal vary
488 with sampling site and date, and net removal rate is faster in Basin B than in Basin A.
489 Mechanisms that control porewater Hg_T concentrations might include precipitation/dissolution of
490 minerals such as cinnabar ($HgS_{(s)}$) and montroydite ($HgO_{(s)}$) (e.g., Winfrey and Rudd, 1990;
491 Ullrich et al., 2001), Hg adsorption to Fe and Mn oxyhydroxides (e.g., Gobeil and Cossa, 1993;
492 Gagnon et al., 1997; Bloom et al., 1999; Hammerschmidt et al., 2004; Heyes et al., 2004; Turner et
493 al., 2004), Hg adsorption to or coprecipitation with Fe sulfide (e.g., Morse and Luther, 1999;
494 Merritt and Amirbahman, 2007; Jeong et al., 2007; Liu et al., 2008) and Hg reaction with organic
495 matter (e.g., Hammerschmidt and Fitzgerald, 2004; Sunderland et al., 2006; Hollweg et al., 2009).
496

Precipitation of cinnabar ($HgS_{(s,\ cinnabar)}$; reaction 23 in Table 2) is not responsible for the observed net porewater Hg_T removal in Lake Tantaré sediments. This is supported by comparison of the ion activity product (IAP) and the solubility product (K_s), which indicates that, in both basins and at all sampling periods, the porewater, from the sediment−water interface to 10 cm depth, was always undersaturated by more than two orders of magnitude with respect to cinnabar. A similar conclusion can be made for the precipitation of montroydite ($HgO_{(s)}$; reaction 24 in Table 2) with porewater being undersaturated by more than 25 orders of magnitude with respect to this solid. It should be noted that varying the value of "y" between 2 and 7 for the complexes HgS_yOH^- and $Hg(S_y)_2^{2-}$ does not alter our conclusion on the saturation state of porewater with respect to these solids. Goulet et al. (2007) also reported that the porewater of a riverine wetland was undersaturated with respect to these solids.

The presence of Hg in the Fe-rich authigenic material collected on Teflon sheets (Table 3) indicates that some Hg is removed from Basin A porewater by authigenic Fe-ox or its associated organic matter. By multiplying the $\{Hg_T\}$:{Fe} molar ratio measured in the Fe-rich material collected with Teflon sheets by the concentration of authigenic Fe-ox in the top 0.5-cm sediment layer (Table 3), we estimate that, at the most, 1.9×10^{-10} mol g^{-1}, i.e., ~6 % of $\{Hg_T\}$ (3×10^{-9} mol g^{-1}), would be bound to the Fe-ox or to its associated organic matter in this sediment layer. An implicit assumption in that calculation is that the authigenic Fe-ox in the top 0.5-cm layer of the sediment have a similar composition to those collected on the Teflon sheets. In Basin A of Lake Tantaré, strong correlations have been observed between porewater [As] (Couture et al., 2010a) or [Mo] (Chappaz et al., 2008) and [Fe] profiles because these anionic trace elements show a strong coupling with Fe redox recycling and they are not readsorbed quickly when they are released by

dissolution of the Fe-ox. The lack of correlation between the porewater [Hg_T] and [Fe] profiles (Fig. 2 a, b and i, j) could be explained by a weaker involvement of Hg in the Fe redox recycling and/or a fast readsorption of the Hg released following the reductive dissolution of the Fe-ox. Adsorption of Hg onto Fe-ox in Basin B sediments can be ruled out since authigenic Fe-ox are absent or at low concentrations in the sediments of this Basin, due to the seasonally anoxic condition (see Figs 2k, l and 4h). Likewise, removal of porewater Hg_T by adsorption onto Mn oxyhydroxides can be ignored because the slightly acidic condition of the lake prevents the formation of this authigenic phase (Laforte et al., 2005). Thus, adsorption to Fe-ox or its associated organic matter likely occurs in Basin A sediments but is of minor importance and does not alone explain the differences observed between Basins A and B in the distribution of {Hg_T} in the top 5 cm of the sediments (Fig. 4a-b).

Coincidence in space between the zone of Hg_T removal in Basin B (Fig. 3k, l) and the depth interval where porewater was slightly oversaturated with respect to disordered mackinawite ($FeS_{(s, m)}$; equation 37 in Table 2) (see Fig. 3s, t) suggests that the relatively fast removal of Hg_T from porewater in this basin could be explained by its adsorption to or coprecipitation with $FeS_{(s, m)}$. This interpretation would also be consistent with the net Hg_T production in July 2007 in Basin B (Fig. 3l) which corresponds to a depth interval (6-10 cm) where porewater was undersaturated with respect to $FeS_{(s, m)}$ (Fig. 3t). However, this mechanism would explain neither the net porewater Hg_T removal in Basin A (zone 1 in Fig. 3i, j), given that porewater was undersaturated with respect to $FeS_{(s, m)}$ (Fig. 3q, r), nor the porewater Hg_T production in Basin B in October 2006 (zone 2; 4-9 cm depth), given that porewater was slightly supersaturated with respect to $FeS_{(s, m)}$. However, in all

these latter cases, where very low [Hg_T] were modeled, the R_{net}^{Hg} values were small and, arguably, could be modeling artifacts.

As a last point, removal of porewater Hg_T by reduced sulfur functional groups on organic matter cannot be dismissed, especially in Basin B. Indeed, our data indicate that relatively high concentrations of sulfur are present (Fig. 4p) over the depth interval where Hg_T is removed from porewater, and, as previously stated in section 3.2, most of the S could be organically-bound. Several studies have speculated that sulfur groups in sediment humic substances could bind Hg (Ravichandran, 2004; Skyllberg, 2008), and such binding has been shown by spectroscopic techniques (XANES) to occur at reduced sulfur sites present in soil humic substances (Xia et al., 1999). There is growing evidence that humic substances become sulfidized in anoxic sediments (e.g., Canfield et al., 1998; Einsield et al., 2008). Also, several studies in coastal marine sediments (e.g., Bloom et al., 1999; Hammerschmidt and Fitzgerald, 2004 and 2006a; Sunderland et al., 2006; Hollweg et al., 2009) have shown a significant correlation between log K_D^{Hg} and $\{C_{org}\}$ or between $\{Hg_T\}$ and $\{C_{org}\}$, which were taken as an indication that Hg was bound to organic matter. We did not observe such correlations, perhaps due to the small depth variation in $\{C_{org}\}$ in the two basins.

Thus, it can be concluded that pure Hg mineral phases do not form in Lake Tantaré sediments and that Hg_T adsorption onto Fe-ox occurs to a limited extent. Moreover, our data do not allow us to demonstrate unambiguously whether Hg_T associations with Fe sulfide phases or sulfidized organic matter are important processes controlling porewater Hg_T concentrations in the lacustrine

anoxic sediments. Additional field and laboratory work are clearly needed to better identify the reactions involving Hg_T in the sediments.

4.2. Modeling the [MeHg] profiles

Fitting of the average (n = 3) porewater [MeHg] profiles in each basin and sampling date and the zones of [MeHg] production or consumption are displayed in Fig. 3m-p whilst the values of the net reaction rates (R_{net}^{MeHg}) are given in Table 5 for each zone numbered downward from the sediment−water interface. In calculating the average [MeHg], undetectable concentrations were assumed to be half the DL.

In Basin A, the code PROFILE defined for September 2005 (Fig. 3m) a zone of slow net MeHg consumption (zone 1) in the first 5 cm below the sediment–water interface ($R_{net}^{MeHg} = -0.2 \times 10^{-21}$ mol cm^{-3} s^{-1}) above a zone of about the same thickness where MeHg was slowly produced (zone 2; $R_{net}^{MeHg} = 0.3 \times 10^{-21}$ mol cm^{-3} s^{-1}). For September 2006, PROFILE suggests a different pattern with two zones of net MeHg consumption and of net production (Fig. 3n). However, fitting of the average [MeHg] profile for September 2006 should be taken with caution, due to the high standard deviation on the average [MeHg] values, especially between the sediment−water interface and 5 cm depth, thus reflecting some local heterogeneity. When they are modeled individually, two of the [MeHg] profiles (Fig. 5a and c) yield a R_{net}^{MeHg} -depth pattern consistent with that obtained for the average [MeHg] profile of September 2005 (Fig. 3m). However, the other [MeHg] profile (Fig. 5b) shows a zone of fast net MeHg production ($R_{net}^{MeHg} = 5.2 \times 10^{-21}$ mol cm^{-3} s^{-1}) located between

two consumption zones extending, one from the sediment–water interface to 1.5 cm depth (R_{net}^{MeHg} = -2.0 × 10^{-21} mol cm^{-3} s^{-1}), and another one from 3 to 10 cm depth (R_{net}^{MeHg} = -0.4 × 10^{-21} mol cm^{-3} s^{-1}). It is worth recalling that samples from three peepers were pooled together in order to get enough volume for the MeHg analysis. This averaging procedure likely leads to underestimate the actual spatial heterogeneity in net MeHg production and consumption rates. An important heterogeneity among replicate [MeHg] profiles, as we observed in Lake Tantaré Basin A, was also noticed in the Penobscot River Estuary (Merritt and Amirbahman, 2008). We do not have a clear explanation for this heterogeneity, which did not show in the sediments of the anoxic Basin B, but we speculate that it is related to small scale variations in the activity of benthic animals.

Modeling the average (n = 3) [MeHg] profiles determined in October 2006 and July 2007 in Basin B leads to similar results for the two sampling periods, with an excellent agreement (r^2 = 0.96-0.99) between measured and modeled data (Fig. 3o, p). It shows a 1.5 to 3-cm thick zone where MeHg is consumed relatively fast (zone 1; R_{net}^{MeHg} = -0.9 × 10^{-21} mol cm^{-3} s^{-1} to -3.5 × 10^{-21} mol cm^{-3} s^{-1}) above a zone of much slower net MeHg consumption (zone 2; R_{net}^{MeHg} = -0.01 × 10^{-21} mol cm^{-3} s^{-1} to -0.03 × 10^{-21} mol cm^{-3} s^{-1}). The R_{net}^{MeHg} values for net MeHg removal from Lake Tantaré porewater are slightly lower than those reported by Goulet et al. (2007) in Lake St. Pierre (R_{net}^{MeHg} = -0.1 × 10^{-21} mol cm^{-3} s^{-1} to -12.4 × 10^{-21} mol cm^{-3} s^{-1}) and much lower than those reported by Merritt and Amirbahman (2008) for the highly contaminated Penobscot River-Estuary sediments (R_{net}^{MeHg} = -10 × 10^{-21} mol cm^{-3} s^{-1} to -650 × 10^{-21} mol cm^{-3} s^{-1}).

607 Processes already hypothesized to remove MeHg from porewater include sorption onto Fe-ox
608 (Bloom et al., 1999; Heyes et al., 2004; Hammerschmidt et al., 2004) and Fe sulfides (Miller,
609 2006), interaction with organic matter (e.g., Hammerschmidt and Fitzgerald, 2004; Lambertsson
610 and Nilsson, 2006), and microbially-mediated demethylation reactions (e.g., Oremland et al. 1991;
611 Marvin-Di Pasquale et al., 2000; Benoit et al., 2003). Processes that release MeHg to porewater
612 would be desorption from the solid phases and Hg methylation (e.g., Olson and Cooper, 1974;
613 Compeau and Bartha, 1985; Gilmour et al., 1992; King et al., 2001).
614
615 The {MeHg}:{Fe-ox} molar ratio measured in the Fe-rich material collected with Teflon
616 sheets (Table 3) provides evidence that some MeHg was removed from Basin A porewater by
617 authigenic Fe-ox or its associated organic matter. By multiplying this ratio by the {Fe-ox} present
618 in the top 0.5-cm sediment layer (1.55×10^{-3} mol g^{-1}; Table 3), we estimate that 1×10^{-12} mol g^{-1},
619 i.e., about 2 % of total {MeHg} (8×10^{11} mol g^{-1}), would be bound to the Fe-ox or to its associated
620 organic matter in this sediment layer. Such a weak adsorption on the authigenic Fe-ox cannot
621 explain the important {MeHg} enrichment (Fig. 4e) grossly coincident with that of Fe (Fig. 4g)
622 just below the surface of Basin A sediments . As discussed later (section 4.4), most of the MeHg in
623 surface sediments must originate from the settling of MeHg-rich particles; MeHg is then
624 demethylated upon sediment burial since there is no reason to suspect a recent abrupt increase in
625 MeHg production in the water column. If we assume a first-order reaction with respect to {MeHg},
626 we estimate, from the sharp decrease in {MeHg} below the sediment−water interface and 3 cm
627 depth (Fig 4e), a demethylation rate constant of 7×10^{-5} d^{-1}. Hines et al. (2004) reported well-
628 defined down-core decreases in {MeHg}, starting from the sediment surface, in several cores
629 collected from a seepage lake. Using the decrease in MeHg accumulation rate as a function of

630 decadal time shown in their Fig. 7 and their average sediment accumulation rate value of 0.013 g
631 cm^{-2} yr^{-1}, a demethylation rate constant of 4×10^{-5} d^{-1} can be calculated. Rydberg et al. (2008) also
632 reported a decline in {MeHg} with sediment age in the varved sediments of lake Nylandssjön;
633 using the data shown in their Fig. 3a, we calculate a demethylation rate constant of 6×10^{-5} d^{-1}. It
634 is noteworthy that the rate constant values obtained from the data reported for the seepage lake and
635 Lake Nylandssjön are reasonably similar to that obtained for Basin A. Thus, based on the above
636 considerations, adsorption onto authigenic material and/or demethylation should contribute to the
637 net MeHg consumption observed just below the sediment−water interface in Basin A (zone 1 in
638 Fig. 3m and 5a-c).
639
640 In Basin B, the net MeHg removal from porewater (zone 1 in Fig. 3o, p) cannot be ascribed to
641 adsorption onto Fe-ox because there is no evidence for the formation of these oxyhydroxides in
642 this anoxic basin. The MeHg removal zone is however located within the depth interval where
643 porewater was slightly supersaturated with respect to $FeS_{(s,\,m)}$ (Fig. 3s, t), suggesting that MeHg
644 could be adsorbed onto or coprecipitated with iron sulfide. This mechanism would explain the
645 slow production of MeHg between 5 and 10 cm depth in Basin A sediments (Fig. 3m and 5a, c)
646 where porewater were undersaturated with respect to $FeS_{(s,\,m)}$. However, it would not explain, for
647 example, the slow net MeHg consumption between 3 and 10 cm depth observed in Basins A (Fig.
648 5b) and B (Fig. 3p) sediments, which, given the small R_{net}^{MeHg} values, might result from modeling
649 artifacts. Lastly, as previously suggested for Hg_T, and as discussed in other studies (Hintelmann et
650 al., 1997; Karlsson and Skyllberg, 2003), removal of MeHg due to interaction with reduced sulfur
651 functional groups on organic matter cannot be dismissed in Basin B sediments, since a large part of
652 the S_T could be organically-bound.

653

654 The zones of net MeHg production in Basin A porewater (Figs. 3m and 5a-c) always occur at
655 depth intervals where SO_4 is consumed (Fig. 2u-v), thus indicating that methylation by sulfate-
656 reducing bacteria is the likely mechanism of production. Consistent with this mechanism, we do
657 not observe any important MeHg production in Basin B porewater where there is no SO_4
658 consumption (Fig. 2w-x). In the latter basin, MeHg production occurs in the water column, i.e.,
659 where SO_4 reduction occurs (Fig. 2w-x), and then MeHg diffuses across the sediment−water
660 interface. Eckley et al. (2005) have shown that MeHg is formed and accumulates in anoxic
661 hypolimnetic lake waters. Laboratory experiments with pure cultures or with Hg-spiked sediments
662 have shown repeatedly the involvement of sulfate reducing bacteria in Hg methylation (e.g. Olson
663 and Cooper, 1974; Compeau and Bartha, 1985; Gilmour et al., 1992; Benoit et al., 2003). MeHg
664 desorption or its release by dissolution of solid phases to which it was bound could also contribute
665 to the net MeHg production, but we have no evidence that these mechanisms are important in Lake
666 Tantaré sediments.

667

668 From the above observations, a general equation for R_{net}^{MeHg} can be:

669

670 $$R_{net}^{MeHg} = R_{ads}^{MeHg} + R_{demethyl}^{MeHg} + R_{methyl}^{Hg} \quad (3)$$

671

672 where R_{ads}^{MeHg} represents the rate of MeHg removal from porewater by adsorption onto Fe-ox, Fe
673 sulfide or organic matter, whereas $R_{demethyl}^{MeHg}$ and R_{methyl}^{Hg} are the rates of MeHg demethylation and Hg
674 methylation, respectively. Estimations of field-derived methylation and demethylation rate
675 constants can be obtained when simplifying assumptions are made.

676 If we assume, for the net consumption zone of dissolved MeHg just below the sediment−water
677 interface in Basins A and B (Figs. 3m, o-p and 5), that R_{ads}^{MeHg} and R_{methyl}^{MeHg} can be neglected in Eq.
678 (3), and that demethylation rate is first order with respect to [MeHg], then:
679
680 $$R_{net}^{MeHg} = R_{demethyl} = -\phi\, k_{demethyl}[MeHg]_{av} \quad (4)$$
681
682 where $k_{demethyl}$ (d^{-1}) is the apparent first-order rate constant for demethylation and the subscript "*av*"
683 indicates that the average value over the thickness of the zone is taken into account because R_{net}^{MeHg}
684 is a piecewise constant function. On this basis, we calculate that $k_{demethyl}$ varies between 0.04 d^{-1}
685 and 0.3 d^{-1} in Basin A and between 0.1 d^{-1} and 0.8 d^{-1} in Basin B. These field-derived rate constant
686 values are slightly lower than that (1.1 d^{-1}) reported by Merritt and Amirbahman (2008) for the
687 Penobscot River estuary. They can also be compared with those recently obtained in laboratory
688 experiments where sediments or lake water samples were simultaneously spiked with low amounts
689 of Hg(II) and MeHg labelled with different stable Hg isotopes and incubated. These experiments
690 allowed the rate constants to be determined simultaneously for the MeHg demethylation and Hg
691 methylation processes. The laboratory-derived $k_{demethyl}$ values reported vary between 0.4 d^{-1}-0.5 d^{-1}
692 for lake sediments (Hintelmann et al., 2000), 0.02 d^{-1}-0.2 d^{-1} for estuarine sediments (Rodriguez
693 Martin-Doimeadios et al., 2004) and 0.03 d^{-1}-0.05 d^{-1} for lake water (Eckley et al., 2005). Thus,
694 our $k_{demethyl}$ values fall within the range reported for these various aquatic environments.
695 Hintelmann et al. (2000) have shown that the rate constants for MeHg demethylation obtained by
696 this approach do not depend on the chemical form of the MeHg spike, i.e., that the MeHg tracer
697 behaves similarly to the MeHg produced in the natural environment studied. It should be noted that

698 the MeHg demethylation rate constant (7 x 10^{-5} d^{-1}) calculated from the decrease with depth of the
699 {MeHg} in Basin A sediments (Fig. 4e) is much lower than the values obtained by modeling the
700 porewater profiles. It indicates that MeHg in the solid phase is not at equilibrium with the
701 dissolved MeHg. We hypothesize that solid-phase MeHg was already incorporated within
702 sediment particles (e.g., phytoplankton, bacteria) when they were deposited and not simply
703 adsorbed onto them; demethylation of MeHg was then controlled by sediment particle degradation.
704 The presence of measurable {MeHg} in Basin A and B sediments (Fig. 4e, f) at depths where SO_4
705 is exhausted supports the slow demethylation of solid phase MeHg. Indeed, methanogenic bacteria
706 have not been reported to methylate Hg. Also, Hintelmann et al. (2000) have shown that amending
707 sediments with sulfide prevents MeHg demethylation.
708
709 If we assume, for the zone of net porewater MeHg production below that of consumption in
710 Basin A, that R_{ads}^{MeHg} and $R_{demethyl}^{MeHg}$ can be neglected in Eq. (3), we obtain:
711
712 $$R_{net}^{MeHg} = R_{methyl}^{Hg} = \phi k_{methyl}[Hg_T]_{av} \quad (5)$$
713
714 where k_{methyl} (d^{-1}) is the apparent first-order rate constant for Hg methylation. It should be noted
715 that the Hg methylation rate is expressed in term of [Hg_T] to allow comparison with k_{methyl} values
716 reported in Hg-spiked laboratory experiments. Our field-derived k_{methyl} values calculated using Eq.
717 (5) range between 0.006 d^{-1} and 0.1 d^{-1}. To the best of our knowledge, no other study has reported
718 field-derived k_{methyl} values. However, laboratory-derived values of this rate constant have been
719 obtained in the double spike experiments described above; they vary from 0.001 d^{-1} to 0.02 d^{-1} for

720 lake sediments (Hintelmann et al., 2000), 0.001 d^{-1} to 0.03 d^{-1} for estuarine sediments (Rodriguez
721 Martin-Doimeadios et al., 2004) and 0.01 d^{-1} to 0.09 d^{-1} for lake water (Eckley et al., 2005). Thus,
722 our field-derived values are of similar magnitude to those obtained in laboratory assays. Such
723 comparison should, however, be taken with caution since the chemical form of the Hg(II) spike
724 can affect the Hg methylation rate, i.e., the Hg(II) spiked could be more available to methylation
725 than the ambient Hg (Hintelmann et al., 2000).
726
727 **4.3. Effect of diagenesis on the solid-phase Hg_T concentrations**
728
729 In environments where sediment mixing is negligible, the measured Hg_T in a sediment layer
730 represents the sum of the Hg_T concentration in the settling particles at deposition time and of the
731 Hg_T concentration released from or added to the sediments during burial. The latter fraction of Hg_T
732 in the sediments, hereafter called diagenetic Hg_T (Hg_{diag}), can be quantified as follows. Equation
733 (6) is first used to relate the removal/production rate of Hg_T to that of Hg_T gain/loss (Laforte
734 et al., 2005; Chappaz et al., 2010):
735
736 $$R_{net}^{Hg} = \phi\left(\frac{d\,Hg_T}{dt}\right)_{reaction} = -m\left(\frac{d\,Hg_T}{dt}\right)_{reaction} \quad (6)$$
737
738 where *m* is the dry bulk density (g cm^{-3} of whole sediment) and the subscript "reaction" indicates
739 reaction rates in solid and solution phases. From Eq. (6), we can then obtain:
740

$$d\left[Hg_T\right] = -\frac{R_{net}^{Hg}}{m}dt = -\frac{R_{net}^{Hg}}{mv_s}dx \quad (7)$$

and

$$\left[Hg_{diag}\right] = -\int_{x=0}^{x=x_i}\frac{R_{net}^{Hg}}{mv_s}dx \approx -\sum_{x=0}^{x=x_i}\frac{R_{net}^{Hg}}{mv_s}\Delta x \quad (8)$$

where v_s is sedimentation rate (cm s^{-1}; Table 1) and x_i is the depth of the sediment layer (maximum depth corresponds to the deepest horizon of collected porewater samples, i.e. 10 cm).

Calculations made with Eq. (8) show that $[Hg_{diag}]$ represents at the most 0.02 nmol g^{-1} (0.9% of $[Hg_T]$) and 0.11 nmol g^{-1} (3.8% of $[Hg_T]$) in Basins A and B, respectively. These concentrations are within our analytical precision (5%). We therefore conclude that post-depositional redistribution of Hg in Lake Tantaré sediments is negligible and that the measured $[Hg_T]$ profiles reflect Hg concentrations in the settling particles at deposition time and not diagenesis.

4.4. Present-day inputs of Hg_T and MeHg to the sediments

The present-day total flux responsible for Hg_T accumulation in the sediments (J_{Acc}^{Hg}) of Lake Tantaré Basin A is the sum of the fluxes of Hg_T deposited at the sediment surface with settling

761 particles (J_{Dep}^{Hg}) and those of dissolved Hg_T transported across the sediment−water interface by
762 molecular diffusion (J_D^{Hg}), bioirrigation (J_I^{Hg}) and bioturbation (J_B^{Hg}):
763
764 $$J_{Acc}^{Hg} = J_{Dep}^{Hg} + J_D^{Hg} + J_I^{Hg} + J_B^{Hg} \quad (9)$$
765
766 In the seasonally anoxic Basin B, J_{Acc}^{Hg} can be reduced to:
767
768 $$J_{Acc}^{Hg} = J_{Dep}^{Hg} + J_D^{Hg} \quad (10)$$
769
770 The present-day values of J_{Dep}^{Hg} for the two basins were obtained by multiplying the sediment mass
771 accumulation rate (ω; mg cm^{-2} yr^{-1}) obtained from the ^{210}Pb geochronology for the top 0.5 cm
772 sediment layer by the measured Hg_T in that layer, which was shown previously (section 4.3) to
773 represent Hg concentration in settling particles. The values of J_D^{Hg}, J_I^{Hg} and J_B^{Hg} were calculated
774 with the code PROFILE (Table 4). The flux of dissolved Hg_T is on the order of 0.8×10^{-21} mol cm^{-2} s^{-1} and 40×10^{-21} mol cm^{-2} s^{-1} in Basins A and B, respectively, representing less than 9% of J_{Acc}^{Hg}
776 (Table 4). Thus, most of the Hg_T is deposited to sediment surface with settling particles, a
777 conclusion that is consistent with the negligible contribution of Hg_{diag} to the measured Hg_T.
778
779 Similarly, present-day fluxes of MeHg can be calculated with Eqs. (9) and (10), where Hg
780 fluxes were replaced by MeHg fluxes (Table 5). The results indicate that, in Basin A, most (>97%)
781 of the MeHg measured at the sediment surface is at the present time deposited with settling

particles. This conclusion is consistent with our previous calculations (see section 4.2) showing that less than 2% of $\{MeHg\}$ in the top sediment layer (0-0.5 cm) is associated with authigenic Fe-ox and its associated organic matter. In contrast, in Basin B, the diffusive flux of MeHg into the sediments (J_D^{MeHg}) is of similar magnitude to that of MeHg deposition with settling particles (J_{Dep}^{MeHg}). Therefore, sediments of both Basins A and B act as a sink for water column MeHg.

4.5. Recent history of anthropogenic Hg deposition

Interpretation of $\{Hg_T\}$ profiles in terms of Hg emission chronology is complex because diagenetic reactions, variations in sediment mass accumulation rate (ω), lake internal processes, as well as variations in Hg inputs from the watershed also contribute to shape the $\{Hg_T\}$ profiles. In Lake Tantaré Basins A and B sediments, as in other lake sediments (Fitzgerald et al., 1998; Lockhart et al., 2000; Rydberg et al., 2008), diagenetic reactions do not appear to affect the $\{Hg_T\}$ records significantly. In the following discussion, it is thus assumed that they also have a negligible influence on Lakes Bédard and Holland $\{Hg_T\}$ records. In order to take into account variations in ω, the results can be expressed as fluxes (pmol cm^{-2} yr^{-1}). The flux of anthropogenic Hg at the coring sites ($J^{Hg-Anth}$; see insets in Fig. 6a-c) is incidentally given by the following equation:

$$J^{Hg-Anth} = Hg_T - Hg_{T\ 1850}\ \omega \qquad (11)$$

where $Hg_{T\ 1850}$ is the average pre-1850 Hg_T. Despite differences in the magnitude of the fluxes, the $J^{Hg-Anth}$ profiles become quite similar in shape in Basins A and B (see inset in Fig. 6a), in sharp contrast to the Hg_T profiles (Fig 4a, b). Lastly, in order to attenuate the effects of lake specific processes, such as sediment focusing and loss of material via the lake outflow, $J^{Hg-Anth}$ has been corrected as follows (Kada and Heit, 1992):

$$J_{Cor}^{Hg-Anth} = J^{Hg-Anth} \times \left(\frac{I_{Atm}^{210Pb}}{I_{Sed}^{210Pb}} \right) \quad (12)$$

where $J_{Cor}^{Hg-Anth}$ is the flux of anthropogenic Hg corrected for the internal lake processes, I_{Sed}^{210Pb} is the inventory of unsupported ^{210}Pb in the sediment cores (Table 1) and I_{Atm}^{210Pb} is the cumulative atmospheric input of ^{210}Pb, which can be assumed to be identical to the average inventory of ^{210}Pb unsupported by the radioactive decay of ^{226}Ra in soils of the Precambrian Shield in Eastern Ontario (0.44 Bq cm^{-2}; Cornett et al., 1984). The implicit assumption to this frequently applied correction used to interpret the Hg_T records in lake sediments (e.g. Engstrom and Swain, 1997; Lamborg et al., 2002; Perry et al., 2005; Sunderland et al., 2008; Muir et al., 2009; Yang et al., 2010), is that transport of Hg to the sediment is similar to that of unsupported ^{210}Pb. Such an assumption is reasonable considering that both Hg and ^{210}Pb are particle-reactive elements. We infer that the $J_{Cor}^{Hg-Anth}$ chronologies reflect essentially variations in atmospheric Hg emissions and watershed contributions of previously deposited atmospheric Hg.

823 The chronological variations in $J_{Cor}^{Hg-Anth}$ for the past 125 years are displayed in Fig. 6 for all
824 study lakes. An interesting feature resulting from this data treatment is the good match between the
825 $J_{Cor}^{Hg-Anth}$ chronologies of Lake Tantaré Basins A and B (Fig. 6a). It should be noted that this good
826 match is not compromised by the fact that Hg accumulation in Basin B sediments is presently
827 incomplete due to the current diffusion of dissolved Hg_T into the sediments (Fig. 3k-l) and its
828 fixation over the top 5 cm of sediments. Indeed, calculations reveal that this process would
829 increase the values of $J_{Cor}^{Hg-Anth}$ by less than 6% if diffusion continues at the same rate until the
830 sediment is buried below 5 cm depth. The good match among the $J_{Cor}^{Hg-Anth}$ records of the two
831 basins supports our finding regarding the negligible effect of diagenetic reactions on the Hg_T
832 concentrations in Lake Tantaré sediments. It also suggests that normalization based on the ^{210}Pb
833 inventory is a valuable approach to correct Hg_T records for lake specific processes.
834
835 The reconstructed records of $J_{Cor}^{Hg-Anth}$ for Lake Tantaré Basins A and B reveal that this flux
836 significantly increased since the end of the 19th Century, reached a maximum in the early 1970s
837 (~14 pmol cm^{-2} yr^{-1}), and then slightly decreased by about 15% during the next 30 years. This
838 temporal trend is coherent with that observed in other studies using lake sediments as archive of
839 environmental contamination in North America (e.g. Engstrom and Swain, 1997; Kamman and
840 Engstrom, 2002; Perry et al., 2005; Biester et al., 2007; Muir et al., 2009). The increase in $J_{Cor}^{Hg-Anth}$
841 from the end of the 19th Century to the early 1970s was attributed to the progressive escalation of
842 industrial activity during that time period in North America (Engstrom and Swain, 1997; Pirrone et
843 al., 1998). Its decline, after the 1970s, was attributed to implementation of new technologies to
844 reduce contaminant emissions at their source, particularly in coal-fired power plants (Pacyna et al.,

2006), but also to the political will to diminish the use of Hg in industrial and commercial products in the U.S., which apparently decreased by more than 75% between 1988 and 1996 (Engstrom and Swain, 1997; USEPA, 1997). It should be noted that a mere interpretation of the Hg_T record in Basin A sediments would have suggested an increase after the 1970s of anthropogenic Hg deposition rather than a decrease.

The present-day value of $J_{Cor}^{Hg-Anth}$ in Basins A and B (~12 pmol cm^{-2} yr^{-1}) is in the lower range of values found in other studies on the distribution of Hg_T in dated lake sediment cores fromEastern North America (5-30 pmol cm^{-2} yr^{-1}; Perry et al., 2005; Muir et al., 2009). On the other hand, it is higher than the annual mean values of atmospheric Hg deposition rate due to precipitations at two Southern Québec sites between 1996 and 2006 (2-4 pmol cm^{-2} yr^{-1}; VanArsdale et al., 2005; NADP, 2010). This discrepancy between $J_{Cor}^{Hg-Anth}$ and the wet atmospheric deposition of Hg cannot only be due to the dry atmospheric Hg deposition which should amount to about 30% of wet Hg deposition (Lamborg et al., 1995; Selvendiran et al., 2009). It rather suggests that an important part of anthropogenic Hg_T accumulating in Lake Tantaré sediments is due to watershed inputs of previously deposited atmospheric Hg (e.g. Swain et al., 1992; Grigal, 2002).

Fig. 6b shows that $J_{Cor}^{Hg-Anth}$ has increased in Lake Bédard from the end of the 19th century to the early 1970s, as in Lake Tantaré, but at a much lower rate, which could be attributed at least partly to a lower Hg contribution from the watershed. It is noteworthy that the catchment area is about 25 times smaller in Lake Bédard than in Lake Tantaré. Indeed, several authors have found a significant correlation between the Hg deposition flux in lake sediments and the catchment area or

868 the catchment/lake area ratio (e.g. Swain et al., 1992; Kamman and Engstrom, 2002; Mills et al.,
869 2009). Moreover, the type of biomass, the soil composition, and human disturbances in the
870 watershed might also have a strong influence on Hg export from the watershed to the lake
871 sediments (e.g. Grigal, 2002; Kainz and Lucotte, 2006; Engstrom et al., 2007; Mills et al., 2009).
872 The Lake Tantaré catchment has a mixed forest of St. Lawrence Lowlands (maple, yellow birch)
873 and boreal forest tree species (fir, spruce, white birch; Payette et al., 1990), while vegetation of
874 Lake Bédard catchment is typical of that of the boreal forest (white birch, balsam fir, white spruce,
875 http://www.ffgg.ulaval.ca/index.php?id=346). The importance of the watershed contribution in Hg
876 is further supported by the presence of a $J_{Cor}^{Hg-Anth}$ peak (~7.4 pmol cm^{-2} yr^{-1}) in the early 1970s,
877 which occurred concurrently with a 4-fold increase in ω values which can likely be associated to
878 the construction of a small forest road in the catchment in the late 1960s. We, however, have no
879 clear explanation for the $J_{Cor}^{Hg-Anth}$ increase in Lake Bédard after ~1990 which is not correlated with
880 an increase in ω.
881
882 In Lake Holland (Fig. 6c), $J_{Cor}^{Hg-Anth}$ increased slowly from the end of the 19th century to the
883 early 1950s and more sharply after this time horizon reaching a maximum value of ~10.3 pmol cm^{-}
884 ^{2} yr^{-1} in the early 1990s, and then progressively decreased by about 50 %. This trend clearly shows
885 the imprint of the nearby Murdochville non-ferrous metal smelter. Production at the smelter began
886 in 1950, steadily increased until its temporary shut down during the 1980s. After the
887 implementation of new technologies to reduce contaminant emissions into the atmosphere, it
888 restarted again in 1989 until the smelter was definitely closed in April 2002. However, the fact that
889 the maximum value of $J_{Cor}^{Hg-Anth}$ is observed few years after the smelter was temporary shutdown
890 indicates that part of the anthropogenic Hg accumulating in Lake Holland sediments was initially

deposited on the watershed and retained for some time in the watershed soils and biomass. Thus, the response of atmospheric deposition of Hg into Lake Holland was delayed by about 10 years; such a delay is consistent with what has been suggested in other studies (Meili et al., 2003; Perry et al., 2005; Harris et al., 2007; Mills et al., 2009),

5. CONCLUSIONS

We have shown that applying thermodynamic and kinetic modeling to field measurements of Hg_T, MeHg and ancillary parameters in sediments and porewaters helps understanding Hg_T and MeHg dynamics in sediments. Hence, we provide evidence that pure Hg mineral phases do not form in the sediments and that Hg_T and MeHg adsorption onto authigenic Fe-ox is of minor importance; however, the assessment of Hg_T and MeHg association with Fe sulfide phases or sulfidized organic matter would require additional field and laboratory measurements. Application of the reaction-transport model to the porewater Hg_T profiles indicates that post-depositional Hg_T redistribution negligibly affects the measured Hg_T profiles in Lake Tantaré sediments, a lake that is representative of many other Canadian Shield lakes. Thus, the measured sediment Hg_T profiles reflect the chronology of Hg_T deposition at the sampling site. Comparison of the results from the two Lake Tantaré basins indicates that normalisation with ^{210}Pb inventories is both appropriate and necessary to correct the sediment Hg_T data for internal lake processes. We also provide field evidence that Hg methylation occurs only when SO_4 is consumed. Use of the inverse modeling approach to interpret the porewater MeHg profiles yields estimates of rate constants for the formation and degradation of MeHg in the sediments; these field-derived rate constants are of

914 similar magnitude as the recent laboratory-derived rate constants obtained by incubating sediments
915 with Hg spikes labelled with stable Hg isotopes. Our results also reveal that sediments act as a sink
916 for MeHg, that most of the MeHg accumulates in sediments deposited under oxic conditions in
917 association with settling particles and that solid-phase MeHg is slowly degraded subsequent to
918 deposition.
919

920 **ACKNOWLEDGMENTS**

921

922 Financial support from the Natural Sciences and Engineering Research Council of Canada and
923 the Fonds de Recherche sur la Nature et les Technologies du Québec are acknowledged. We thank
924 L. Rancourt, R. Rodrigue, P. Fournier and B. Averty for their technical assistance and two
925 anonymous reviewers for critical comments. Permission from the Québec Ministère de
926 l'Environnement to work in the Tantaré Ecological Reserve and from Faune et Parcs Québec to
927 work in the Aiguebelle Provincial Park are gratefully acknowledged.
928

REFERENCES

Alfaro-De La Torre M. C. and Tessier A. (2002) Cadmium deposition and mobility in the sediments of an acidic oligotrophic lake. *Geochim. Cosmochim. Acta* **66**, 3549-3562.

Belzile N., De Vitre R. R. and Tessier A. (1989) *In situ* collection of diagenetic iron and manganese oxhydroxides from natural sediments. *Nature* **340**, 376-377.

Belzile N., Lang C.-Y., Chen Y.-W. and Wang M. (2008) The competitive role of organic carbon and dissolved sulfide in controlling the distribution of mercury in freshwater lake sediments. *Sci. Total Environ*. **405**, 226-238.

Benoit J. M., Gilmour C. C., Heyes A., Mason R. P. and Miller C. L. (2003) Geochemical and biological controls over methylmercury production and degradation in aquatic ecosystems. In: Cai Y. and Braids O. C., (Eds.) *Biogeochemistry of Environmentally Important Trace Elements*, ACS Symp. Ser. **835,** 262-297. American Chemical Society, Washington D.C.

Berg P., Risgaard-Petersen N. and Rysgaard S. (1998) Interpretation of measured concentration profiles in sediment porewater. *Limnol. Oceanogr.* **43**, 1500-1510.

Berner R. A. (1980) *Early Diagenesis: a Theoretical Approach*. Princeton University Press.

Biester H., Bindler R., Martinez-Cortinas A. and Engstrom D. R. (2007) Modeling the past atmospheric deposition of mercury using natural archives. *Environ. Sci. Technol.* **41**, 4851-4860.

Bloom N. S. and Fitzgerald W. F. (1988) Determination of volatile mercury species at picogram level by low temperature gas chromatography with cold-vapour atomic fluorescence detection. *Anal. Chim. Acta* **28**, 151-161.

951 Bloom N. S., Gill G. A., Capellino S., Dobbs C., McShea L., Driscoll C., Mason R. and Rudd J.
952 (1999) Speciation and cycling of mercury in Lavaca Bay. *Environ. Sci. Technol.* **33**, 7-13.
953 Boudreau B. P. (1984) On the equivalence of nonlocal and radial-diffusion models for porewater
954 irrigation. *J. Mar. Res.* **42**, 731-735.
955 Boudreau B. P. (1997) *Diagenetic Models and their Implementation.* Springer-Verlag.
956 Buffle J. (1988) *Complexation Reactions in Aquatic Systems*. Ellis Horwood Ltd.
957 Canfield D., Boudreau B. P., Mucci A. and Gundersen J. K. (1998) The early diagenetic formation
958 of organic sulfur in the sediments of Mangrove Lake, Bermuda. *Geochim. Cosmochim.*
959 *Acta* **62**, 767-781.
960 Carignan R., St-Pierre S. and Gächter R. (1994) Use of diffusion samplers in oligotrophic lake
961 sediments: effects of free oxygen in sampler material. *Limnol. Oceanogr.* **39**, 468-474.
962 Chappaz A., Gobeil C. and Tessier A. (2008) Geochemical and anthropogenic enrichments of Mo
963 in sediments from perennially oxic and seasonally anoxic lakes in Eastern Canada.
964 *Geochim. Cosmochim. Acta* **72**, 170-184.
965 Chappaz A., Gobeil C. and Tessier A. (2010) Controls on uranium distribution in lake sediments.
966 *Geochim Cosmochim. Acta* **74**, 203-214.
967 Compeau G. C. and Bartha R. (1985) Sulfate-reducing bacteria: principal methylators of mercury
968 in anoxic estuarine sediment. *Appl. Environ. Microbiol.* **50**, 498-502.
969 Cornett R. J., Chant L. and Link D. (1984) Sedimentation of Pb-210 in Laurentian Shield lakes.
970 *Water Poll. Res. J. Canada* **19**, 97-109.
971 Cossa D., Coquery M., Nakhlé K. and Claisse D. (2002) Dosage du mercure total et du
972 monométhylmercure dans les organismes et les sédiments marins. Editions Ifremer2-
973 84433-105-X; 27pp.

974 Cossa D., Averty B. and Pirrone N. (2009) The origin of methylmercury in open Mediterranean
975 waters. *Limnol. Oceanogr*. **54**, 837-844.
976 Couture R.-M., Gobeil C. and Tessier A. (2008) Chronology of atmospheric deposition of arsenic
977 inferred from reconstructed sedimentary records. *Environ. Sci. Technol*. **42**, 6508-6513.
978 Couture R.-M., Gobeil C. and Tessier A. (2010a) Arsenic, iron and sulfure co-diagenesis in lake
979 sediments. *Geochim. Cosmochim. Acta* **74**, 1238-1255.
980 Couture R.-M., Shafei B., Van Cappellen P., Tessier A. and Gobeil C. (2010b) Non-steady state
981 modeling of arsenic diagenesis in lake sediments. *Environ. Sci. Technol*. **44**, 197-203.
982 De Robertis A., Foti C., Patane G. and Sammartano S. (1998) Hydrolysis of $(CH_3)Hg^+$ in different
983 ionic media: salt effects and complex formation. *J. Chem. Eng. Data* **43**, 957-960.
984 Eckley C. S., Watras C. J., Hintelmann H., Morrison K., Kent A. D. and Regnell O. (2005)
985 Mercury methylation in the hypolimnetic waters of lakes with and without connection to
986 wetlands in northern Wisconsin. *Can. J. Fish. Aquat. Sci.* **62**, 400-411.
987 Einsield F., Mayer B. and Schäfer T. (2008) Evidence for incorporation of H_2S in groundwater
988 fulvic acids from stable isotope ratios and sulfur K-edge X-ray absorption near edge
989 structure spectroscopy. *Environ. Sci. Technol*. **42**, 2439-2444.
990 Engstrom D. R., Balogh S. J. and Swain E. B. (2007) History of mercury inputs to Minnesota
991 lakes: influences of watershed disturbance and localized atmospheric deposition. *Limnol.*
992 *Oceanogr.* **52**, 2467-2683.
993 Engstrom D. R. and Swain E. B. (1997) Recent declines in atmospheric mercury deposition in the
994 Upper Midwest. *Environ. Sci. Technol.* **31**, 960-967.

995 Ethier A. L. M., Scheuhammer A. M., Blais J. M., Paterson A. M., Mierle G., Ingram R. and Lean
996 D. R. S. (2010) Mercury empirical relationships in sediments from three Ontario lakes. *Sci.*
997 *Total Environ.* **408**, 2087-2095.
998 Evers D. C., Kaplan J. D., Meyer M. W., Reaman P. S., Braselton W. E., Major A., Burgess N. and
999 Scheuhammer A. M. (1998) Geographic trend in mercury measured in common loon
1000 feathers and blood. *Environ. Toxicol. Chem.* **17**, 173-183.
1001 Feyte S., Tessier A., Gobeil C. and Cossa D. (2010) *In situ* adsorption of mercury, methylmercury
1002 and other elements by iron oxyhydroxides and organic matter in lake sediments. *Appl.*
1003 *Geochem.* **25**, 984-995.
1004 Fitzgerald W. F., Engstrom D. R., Lamborg C. H., Tseng C.-M., Balcom P. H. and
1005 Hammerschmidt C. R. (2005) Modern and historic atmospheric mercury in Northern
1006 Alaska: global sources and Arctic depletion. *Environ. Sci. Technol.* **39**, 557-568.
1007 Fitzgerald W. F., Engstrom D. R., Mason R. P. and Nater E. A. (1998) The case for atmospheric
1008 mercury contamination in remote areas. *Environ. Sci. Technol.* **32**, 1-7.
1009 Fitzgerald W. F., Lamborg C. H. and Hammerschmidt C. R. (2007) Marine biogeochemical
1010 cycling of mercury. *Chem. Rev.* **107**, 641-662.
1011 Fortin D., Leppard G. G. and Tessier A. (1993) Characteristics of lacustrine diagenetic iron
1012 oxyhydroxides. *Geochim. Cosmochim. Acta* **57**, 4391-4404.
1013 Gagnon C., Pelletier É. and Mucci A. (1997) Behavior of anthropogenic mercury in coastal marine
1014 sediments. *Mar. Chem.* **59**, 159-176.
1015 Gallon C., Tessier A., Gobeil C. and Alfaro-De La Torre M. C. (2004) Modeling diagenesis of lead
1016 in sediments of a Canadian Shield lake. *Geochim. Cosmochim. Acta* **68**, 3531-3545.

1017 Gill G. A., Bloom N. S., Cappellino S., Driscoll C. T., Dobbs C., McShea L., Mason R. and Rudd
1018 J. W. M. (1999) Sediment-water fluxes of mercury in Lavaca Bay, Texas. *Environ. Sci.*
1019 *Technol.* **33**, 663-669.
1020 Gilmour C. C., Henry E. A. and Mitchell R. (1992) Sulfate stimulation of mercury methylation in
1021 freshwater sediments. *Environ. Sci. Technol.* **26**, 2281-2287.
1022 Gobeil C. and Cossa D. (1993) Mercury in sediments and sediment porewater in the Laurentian
1023 Through. *Can. J. Fish. Aquat. Sci*. **50**, 1794-1800.
1024 Goulet R., Holmes J., Page B., Poissant L., Siciliano S. D., Lean D. R. S., Wang F., Amyot M. and
1025 Tessier A. (2007) Mercury transformations and fluxes in sediments of a riverine wetland.
1026 *Geochim. Cosmochim. Acta* **71**, 3393-3406.
1027 Grigal D. F. (2002) Inputs and outputs of mercury from terrestrial watersheds: a review. *Environ.*
1028 *Rev.* **10**, 1-39.
1029 Gunneriusson L. D., Baxter D. and Emteborg H. (1995) Complexation at low concentrations of
1030 methyl and inorganic mercury(II) to a hydrous goethite (α-FeOOH) surface. *J. Coll. Interf.*
1031 *Sci.* **169**, 262-266.
1032 Hamilton-Taylor J., Willis M., Reynold C. S. (1984) Depositional fluxes of metals and
1033 phytoplankton in Windermere as measured by sediment traps. *Limnol. Oceanogr.* **29**, 695-
1034 710.
1035 Hammerschmidt C. R. and Fitzgerald W. F. (2004) Geochemical controls on the production and
1036 distribution of methylmercury in near-shore marine sediments. *Environ. Sci. Technol.* **38**,
1037 1487-1495.
1038 Hammerschmidt C. R. and Fitzgerald W. F. (2006a) Methylmercury cycling in sediments on the
1039 continental shelf of southern New England. *Geochim. Cosmochim. Acta* **70**, 918-930.

1040 Hammerschmidt C. R. and Fitzgerald W. F. (2006b) Methylmercury in freshwater fish linked to
1041 atmospheric mercury deposition. *Environ. Sci. Technol.* **40**, 7764-7770.
1042 Hammerschmidt C. R., Fitzgerald W. F., Lamborg C. H., Balcom P. H. and Tseng C. M. (2006)
1043 Biogeochemical cycling of methylmercury in lakes and tundra watersheds of Arctic
1044 Alaska. *Environ. Sci. Technol.* **40**, 1204-1211.
1045 Hammerschmidt C. R., Fitzgerald W. F., Lamborg C. H., Balcom P. H. and Visscher P. T. (2004)
1046 Biogeochemistry of methylmercury in sediments of Long Island Sound. *Mar. Chem.* **90**,
1047 31-52.
1048 Hare L., Carignan R. and Huerta-Diaz M. A. (1994) A field study of metal toxicity and
1049 accumulation by benthic invertebrates; implications for the acid-volatile sulfide (AVS)
1050 model. *Limnol. Oceanogr.* **39**, 1653-1668.
1051 Harris R. C., Rudd J. W. M., Amyot M., Babiarz C. L., Beaty K. G., Blanchfield P. J., Bodaly R.
1052 A., Branfireun B. A., Gilmour C. C., Graydon J. A., Heyes A. H. H., Hurley J. P., Kelly C.
1053 A., Krabbenhoft D. P., Lindberg S. E., Mason R. P., Paterson M. J., Podemski C. L.,
1054 Robinson A., Sandilands K. A., Southworth G. R. and St Louis V. L. (2007) Whole-
1055 ecosystem study shows rapid fish-mercury response to changes in mercury deposition. *P.*
1056 *Nat. Acad. Sci.* **104**, 16586-16591.
1057 He T., Lu J., Yang F. and Feng X. (2007) Horizontal and vertical variability of mercury species in
1058 pore water and sediments in small lakes in Ontario. *Sci. Total Environ.* **386**, 53-64.
1059 Heyes A., Miller C. and Mason R. P. (2004) Mercury and methylmercury in Hudson River
1060 sediment: impact of tidal resuspension on partitioning and methylation. *Mar. Chem.* **90**, 75-
1061 89.

1062 Hines N. A., Brezonik P. L. and Engstrom D. R. (2004) Sediment and porewater profiles and
1063 fluxes of mercury and methylmercury in a small seepage lake in northern Minnesota.
1064 *Environ. Sci. Technol.* **38**, 6610-6617.
1065 Hintelmann H., Keppel-Jones K. and Evans R. D. (2000) Constants of mercury methylation and
1066 demethylation rates in sediments and comparison of tracer and ambient mercury
1067 availability. *Environ. Toxicol. Chem.* **19**, 2204-2211.
1068 Hintelmann H., Welbourn P. M. and Evans R. D. (1997) Measurement of complexation of
1069 methylmercury(II) compounds by freshwater humic substances using equilibrium dialysis.
1070 *Environ. Sci. Technol.* **31**, 489-495.
1071 Hollweg T. A., Gilmour C. C. and Mason R. P. (2009) Methylmercury production in sediments of
1072 Chesapeake Bay and the mid-Atlantic continental margin. *Mar. Chem.* **114**, 86-101.
1073 Jay J. A., Morel F. M. M. and Hemond H. F. (2000) Mercury speciation in the presence of
1074 polysulfides. *Environ. Sci. Technol.* **34**, 2196-2200.
1075 Jeong H. Y., Klaue B., Blum J. D. and Hayes K. F. (2007) Sorption of mercuric ion by synthetic
1076 nanocrystalline mackinawite (FeS). *Environ. Sci. Technol.* **41**, 7699-7705.
1077 Kada J. and Heit M. (1992) The inventories of anthropogenic Pb, Zn, As, Cd, and the
1078 radionuclides ^{137}Cs and excess ^{210}Pb in lake sediments of the Adirondack region, USA.
1079 *Hydrobiologia* **246**, 231-241.
1080 Kainz and Lucotte (2006) Mercury concentrations in lake sediments - revisiting the predictive
1081 power of catchment morphometry and organic matter composition. *Water Air Soil Poll.*
1082 **170**, 173-189.

1083 Kainz M., Lucotte M. and Parrish C. C. (2003) Relationships between organic matter composition
1084 and methylmercury content of offshore and carbon-rich littoral sediments in an oligotrophic
1085 lake. *Can J. Fish. Aquat. Sci.* **60**, 888-896.
1086 Kamman N. C. and Engstrom D. R. (2002) Historical and present fluxes of mercury to Vermont
1087 and New Hampshire lakes inferred from ^{210}Pb dated sediment cores. *Atmos. Environ.* **36**,
1088 1599-1609.
1089 Karlsson T. and Skyllberg U. (2003) Bonding of ppb levels of methyl mercury to reduced sulfur
1090 groups in soil organic matter. *Environ. Sci. Technol.* **37**, 4912-4918.
1091 King J. K., Kostka J. E., Frischer M. E., Saunders F. M. and Jahnke R. A. (2001) A quantitative
1092 relationship that demonstrates mercury methylation rates in marine sediments are based on
1093 the community composition and activity of sulfate-reducing bacteria. *Environ. Sci.*
1094 *Technol.* **35**, 2491-2496.
1095 Krabbenhoft D. P., Gilmour C. C., Benoit J. M., Babiarz C. L., Andren A. W. and Hurley J. P.
1096 (1998) Methylmercury dynamics in littoral sediments of a temperate seepage lake. *Can. J.*
1097 *Fish. Aquat. Sci.* **55**, 835-844.
1098 Laforte L., Tessier A., Gobeil C. and Carignan R. (2005) Thallium diagenesis in lake sediments.
1099 *Geochim. Cosmochim. Acta* **69**, 5295-5306.
1100 Lambertsson L. and Nilsson M. (2006) Organic material: the primary control on mercury
1101 methylation and ambient methylmercury concentrations in estuarine sediments. *Environ.*
1102 *Sci. Technol.* **40**, 1822-1829.
1103 Lamborg C. H., Fitzgerald W. F., Damman A. W. H., Benoit J. M., Balcom P. H. and Engstrom D.
1104 R. (2002) Modern and historic atmospheric mercury fluxes in both hemispheres: global and
1105 regional mercury cycling implications. *Global Biogeochem. Cycles* **16**, 51, 1-11.

1106 Lamborg C. H., Fitzgerald W. F., Vandal G. M. and Rolfhus K. R. (1995) Atmospheric mercury in
1107 Northern Wisconsin: source and speciation. *Water Air Soil Poll.* **80**, 189-198.
1108 Leermakers M., Galletti S., De Galan S., Brion N. and Baeyens W. (2001) Mercury in the
1109 Southern North Sea and Scheldt estuary. *Mar. Chem*. **75**, 229-248.
1110 Leermakers M., Baeyens W., Quevauviller P. and Horvat M. (2005) Mercury in environmental
1111 samples: speciation, artifacts and validation. *Trends Anal. Chem.* **24**, 383-393.
1112 Liu J., Valsaraj K. T., Devai I. and DeLaune R. D. (2008) Immobilization of aqueous Hg(II) by
1113 mackinawite (FeS). *J. Hazard. Mater*. **157**, 432-440.
1114 Lockhart W. L., Macdonald R. W., Outridge P. M., Wilkinson P., DeLaronde J. B. and Rudd J. W.
1115 M. (2000) Tests of the fidelity of lake sediment core records of mercury deposition to
1116 known histories of mercury contamination. *Sci. Total Environ.* **260**, 171-180.
1117 Loux N. T. (2007) An assessment of thermodynamic reaction constants for simulating aqueous
1118 environmental monomethylmercury speciation. *Chem. Spec. Bioavailab.* **19**, 183-196.
1119 Malcolm R. L. (1985) Geochemistry of stream fulvic and humic substances. In *Humic Substances*
1120 *in Soil, Sediment and Water. Geochemistry, Isolation and Characterization* (ed. G. R.
1121 Aiken et al.), pp. 181-209. Wiley-Interscience.
1122 Martell A. E. and Smith R. M. (2001) NIST Critically Selected Stability Constants of Metal
1123 Complexes, version 6 Gaithersburg, Maryland: National Institute of Standards and
1124 Technology.
1125 Martell A. E., Smith R. M. and Motekaitis R. J. (2003) NIST critical constants for metal
1126 complexes. NIST Standard Reference Database 46, U.S. Department of Commerce,
1127 National Institute of Standards and Technology, Gaithersburgh, MD.

1128 Marvin-Di Pasquale M. C., Agee J., McGowan C., Oremland R. S., Thomas M., Krabbenhoft D.
1129 and Gilmour C. C. (2000) Methylmercury degradation pathways: a comparison among
1130 three mercury-impacted ecosystems. *Environ. Sci. Technol.* **34**, 4908-4916.
1131 Matisoff G. and Wang X. (1998) Solute transport in sediments by freshwater infaunal bioirrigators.
1132 *Limnol. Oceanogr.* **43,** 1487-1499.
1133 Matisoff G. and Wang X. (2000) Particle mixing by freshwater infaunal bioirrigators: midges
1134 (chironomidae: diptera) and mayflies (ephemeridae: ephemeroptera). *J. Great Lakes Res.*
1135 **26**, 174-182.
1136 Meili M., Bishop K., Bringmark L., Johansson K., Munthe J., Sverdrup H. and De Vries W. (2003)
1137 Critical levels of atmospheric pollution: criteria and concepts for operational modelling of
1138 mercury in forest and lake ecosystems. *Sci. Total Environ.* **304**, 83-106.
1139 Merritt K. A. and Amirbahman A. (2007) Mercury dynamics in sulfide-rich sediments:
1140 geochemical influence on contaminants mobilization within the Penobscot River estuary,
1141 Maine, USA. *Geochim. Cosmochim. Acta* **71**, 929-941.
1142 Merritt K. A. and Amirbahman, A. (2008) Methylmercury cycling in estuarine sediment pore
1143 waters (Penobscot River estuary, Maine, USA). *Limnol. Oceanogr*. **53**, 1064-1075.
1144 Miller C. L. (2006) The role of organic matter in the dissolved phase speciation and solid phase
1145 partitioning of mercury. PhD thesis. University of Maryland, College Park.
1146 Mills R. B., Paterson A. M., Blais J. M., Lean D. R. S., Smol J. P. and Mierle G. (2009) Factors
1147 influencing the achievement of steady state in mercury contamination among lakes and
1148 catchments of south-central Ontario. *Can. J. Fish. Aquat. Sci*. **66**, 187-200.
1149 Morse J. W. and Luther G. W. (1999) Chemical influences on trace metal-sulfide interactions in
1150 anoxic sediments. *Geochim. Cosmochim. Acta* **63**, 3373-3378.

1151 Muir D. C. G., Wang X., Yang F., Nguyen N., Jackson T. A., Evans M. S. D. M., Köck G.,
1152 Lamoureux S., Pienitz R., Smol J. P., Vincent W. F. and Dastoor A. (2009) Spatial trends
1153 and historical deposition of mercury in Eastern and Northern Canada inferred from lake
1154 sediment cores. *Environ. Sci. Technol*. **43**, 4802-4809.
1155 Munthe J., Bodaly R. A., Branfireun B. A., Driscoll C. T., Gilmour C. C., Harris, R, Horvat M.,
1156 Lucotte M. and Malm O. (2007) recovery of mercury-contaminated fisheries. *Ambio* **36**,
1157 33-44.
1158 NADP (2010) Mercury Deposition Network Public Database. http://nadp.sws.uiuc.edu/mdn.
1159 National Atmospheric Deposition Program Office, Illinois State Water Survey, Champaign,
1160 IL.
1161 Newhook R., Hirtle H., Byrne K. and Meek M. E. (2003) Release from copper smelters and
1162 refineries and zinc plants in Canada: Human health exposure and risk characterization. *Sci.*
1163 *Total Environ*. **301**, 23–41.
1164 Olson B. H. and Cooper R. C. (1974) *In situ* methylation of mercury in estuarine sediments.
1165 *Nature* **252**, 682-683.
1166 Oremland R. S., Culberton C. W. and Winfrey M. R. (1991) Methylmercury decomposition in
1167 sediments and bacterial cultures: involvement of methanogens and sulphate reducers in
1168 oxidative demethylation. *Appl. Environ. Microbiol.* **57**, 130-137.
1169 Pacyna E. G., Pacyna J. M., Steenhuisen F. and Wilson S. (2006) Global anthropogenic mercury
1170 emission inventory for 2000. *Atmos. Environ*. **40**, 4048-4063.
1171 Parker J.L. and Bloom N.S. (2005) Preservation and storage techniques for low-level aqueous
1172 mercury speciation. *Sci. Tot. Environ.* **337**, 253-263.

Payette, D. E., Filion L. and Delwaide A. (1990) Disturbance regime of a cold temperate forest as deduced from tree-rings patterns: the Tantaré Ecological Reserve, Quebec. *Can. J. For. Res.* **20**, 1228-1241.

Perry E., Norton S. A., Kamman N. C., Lorey P. M. and Driscoll C. T. (2005) Deconstruction of historic mercury accumulation in lake sediments, Northeastern United States. *Ecotoxicology* **14**, 85-99.

Pirrone N., Allegrini I., Keeler G. J., Nriagu J. O., Rossmann R. and Robbins J. A. (1998) Historical atmospheric mercury emissions and depositions in North America compared to mercury accumulations in sedimentary records. *Atmos. Environ.* **32**, 929-940.

Powell K. J., Brown P. L., Byrne R. H., Gajda T., Hefter G., Sjöberg S. and Wanner H. (2005) Chemical speciation of environmentally significant heavy metals with inorganic ligands. Part 1: The Hg^{2+} - Cl^-, OH^-, CO_3^{2-}, SO_4^{2-}, and PO_4^{2-} aqueous systems. *Pure Appl. Chem.* **77**, 739-800.

Rabenstein D. L., Touranqueau M. C. and Evans C. A. (1976) Proton magnetic resonance and Raman spectroscopic studies of methylmercury(II) complexes of inorganic anions. *Can. J. Chem.* **54**, 2517-2525.

Ramlal P. S., Rudd J. W. M. and Hecky R. E. (1986) Methods for measuring specific rates of mercury methylation and degradation and their use in determining factors controlling net rates of mercury methylation. *Appl. Environ. Microbiol.* **51**, 110-114.

Ravichandran M. (2004) Interactions between mercury and dissolved organic matter - a review. *Chemosphere* **55**, 319-331.

1194 Redfield A. C. (1934) On the proportions of organic derivatives in seawater and their relation to
1195 the composition of plankton. *In*: Daniel, R.J. (Ed.), *James Johnson Memorial Volume*.
1196 Liverpool University Press, Liverpool.
1197 Rickard D. (2006) The solubility of FeS. *Geochim. Cosmochim. Acta* **70**, 5779-5789.
1198 Rodriguez Martin-Doimeadios R. C., Tessier E., Amouroux D., Guyauneaud R., Duran R.,
1199 Caumette P. and Donard O. F. X. (2004) Mercury methylation/demethylation and
1200 volatilization pathways in estuarine sediment slurries using species-specific enriched stable
1201 isotopes. *Mar. Chem.* **90**, 107-123.
1202 Rydberg J., Gälman V., Renberg I. and Bindler R. (2008) Assessing the stability of mercury and
1203 methylmercury in a varved lake sediment deposit. *Environ. Sci. Technol.* **42**, 4391-4396.
1204 Selvendiran P., Driscoll C. T., Montesdeoca M. R., Choi H.-D. and Holsen T. M. (2009) Mercury
1205 dynamics and transport in two Adirondack lakes. *Limnol. Oceanogr*. **54**, 413-427.
1206 Skyllberg U. (2008) Competition among thiols and inorganic sulfides and polysulfides for Hg and
1207 MeHg in wetland soils and sediments under suboxic conditions: illumination of
1208 controversies and implications for MeHg net production. *J. Geophys. Res*. **113**, G00C03,
1209 *doi*: 10.1029/2008JG000745.
1210 Stoichev T., Rodriguez Martin-Doimeadios R. C., Tessier E., Amouroux D. and Donard O. F. X.,
1211 (2004) Improvement of analytical performances for mercury speciation by on-line
1212 derivatization, cryofocussing and atomic fluorescence spectrometry. *Talanta* **62**, 433-438.
1213 Sunderland E. M., Gobas F. A. P. C., Branfireun B. A. and Heyes, A. (2006) Environmental
1214 controls on the speciation and distribution of mercury in coastal sediments. *Mar. Chem*.
1215 **102**, 111-123.

1216 Sunderland E. M., Cohen M. D., Selin N. E. and Chmura G. L. (2008) Reconciling models and
1217 measurements to assess trends in atmospheric mercury deposition. *Environ. Poll*. **156**, 526-
1218 535.
1219 Swain E. B., Engstrom D. R., Brigham M. E., Henning T. A. and Brezonik P. L. (1992) Increasing
1220 rates of atmospheric mercury deposition in midcontinental North America. *Science* **257**,
1221 784-787.
1222 Tiffreau C., Lützenkirchen J. and Behra P. (1995) Modeling the adsorption of mercury(II) on
1223 (Hydr)oxides. 1. Amorphous iron oxide and α-quartz. *J. Coll. Interf. Sci.* **172**, 82-93.
1224 Tipping E. (2002) *Cation Binding by Humic Substances*. Cambridge University Press.
1225 Tipping E. (2007) Modelling the interactions of Hg(II) and methylmercury with humic substances
1226 using WHAM/Model VI. *Appl. Geochem.* **22**, 1624-1635.
1227 Turner A., Millward G. E. and Le Roux S. M. (2004) Significance of oxides and particulate
1228 organic matter in controlling trace metal partitioning in a contaminated estuary. *Mar.*
1229 *Chem.* **88**, 179-192.
1230 Ullrich S. M., Tanton T. W. and Abdrashitova S. A. (2001) Mercury in the aquatic environment: a
1231 review of factors affecting methylation. *Crit. Rev. Environ. Sci. Technol.* **31**, 241-293.
1232 USEPA (1997) *Mercury Study Report to Congress. Volume II: An Inventory of Anthropogenic*
1233 *Emissions in the United States*. EPA-452/R-97-004. U.S. Environmental Protection
1234 Agency. Office of Air Quality & Standards and Office of Research and Development.
1235 USEPA (2002) Method 1631, Revision E: Mercury in water by oxidation, purge and trap, and cold
1236 vapor atomic fluorescence spectrometry. EPA-821-R-02-019. U.S. Environmental
1237 Protection Agency, Office of Water.

USEPA (2007) Method 7473: Mercury in solids and solutions by thermal decomposition, amalgamation, and atomic absorption spectrophotometry, http://www.epa.gov/osw/hazard/testmethods/sw846/pdfs/7473.pdf

VanArsdale A., Weiss J., Keeler G., Miller E., Boulet G., Brulotte R. and Poissant L. (2005) Patterns of mercury deposition and concentration in Northeastern North America (1996-2002). *Ecotoxicology* **14**, 37-52.

Wang F., Tessier A. and Buffle J. (1998) Voltammetric determination of elemental sulfur in pore waters. *Limnol. Oceanogr.* **43**, 1353-1361.

Wang F. and Tessier A. (2009) Zero-valent sulfur and metal speciation in sediment porewaters of freshwater lakes. *Environ. Sci. Technol*. **43**, 7252-7257.

Wedepohl K. H. (1995) The composition of the continental crust. *Geochim. Cosmochim. Acta* **59**, 1217-1232.

Winfrey M. R. and Rudd J. W. M. (1990) Environmental factors affecting the formation of methylmercury in low pH lakes. *Environ. Toxicol. Chem.* **9**, 853-869.

Xia K., Skyllberg U. L., Bleam W. F., Bloom P. R., Nater E. A. and Helmke P. A. (1999) X-ray absorption spectroscopic evidence for the complexation of Hg(II) by reduced sulfur in soil humic substances. *Environ. Sci. Technol.* **33**, 257-261.

Yang H., Battarbee R. W., Turner S. D., Rose N. L., Derwent R. G., Wu G. and Yang R. (2010) Historical reconstruction of mercury pollution across the Tibetan Plateau using lake sediments. *Environ. Sci. Technol.* **44**, 2918-2924.

Table 1. Location and characteristics of the study lakes.

Lake	Tantaré		Bédard	Holland
	Basin A	Basin B		
Geographical coordinates	47°04'N 71°32'W		47°16'N 71°07'W	48°56'N 65°23'W
Geological region	Can. Shield		Can. Shield	Appalachian
Altitude (m)	450		680	475
Lake area (km^2)	1.1		0.045	0.008
Watershed area (km^2)	10.5		0.27	1.3
Sampling depth (m)	15	22	10	11
Redox state of bottom water	Perennially oxic	Seasonally anoxic	Seasonally anoxic	Seasonally anoxic
Sampling dates				
Coring	June 03	June 06	Sept. 04	August 05
Porewater	Sept. 05	Sept. 06	None	None
	Sept. 06	July 07	None	None
pH of bottom water	5.5-5.8	6.6-7.0	6.9-7.0	7.5-7.6
ω (mg cm^{-2} yr^{-1})[a]	4.0-7.3	10.8	2.4-46.8	4.5-15.7
v_s (mm yr^{-1})[a]	0.9-1.3	1.1-1.5	0.5-2.6	0.5-4.4
I_{Sed}^{210Pb} (Bq cm^{-2})[a]	0.37	0.58	0.62	0.61

[a]: ω represents the sediment mass accumulation rate, v_s the sedimentation rate and I_{Sed}^{210Pb} the inventory of unsupported ^{210}Pb in the sediment cores;the data were originally reported in Couture et al. (2008, 2010a).

Table 2. Reactions and their corresponding equilibrium constants (at 25°C and ionic strength = 0) used to update the WHAM 6 database. For the formation of polysulfides complexes, the equilibrium constants have been expressed in terms of dissolved zero-valent S using the reaction 1/8 $S(\alpha)_{8(s)} = S(0)_{aq}$; log K_s = -6.68 (Wang and Tessier, 2009)[a].

No.	Reaction	Log K	References
1	$Hg^{2+} + OH^- = HgOH^+$	10.6	Powell et al. (2005)
2	$Hg^{2+} + 2OH^- = Hg(OH)_2$	22.02	Powell et al. (2005)
3	$Hg^{2+} + 3OH^- = Hg(OH)_3^-$	20.9	Powell et al. (2005)
4	$Hg^{2+} + OH^- + Cl^- = HgOHCl$	18.27	Powell et al. (2005)
5	$Hg^{2+} + Cl^- = HgCl^+$	7.3	Powell et al. (2005)
6	$Hg^{2+} + 2Cl^- = HgCl_2$	14.0	Powell et al. (2005)
7	$Hg^{2+} + 3Cl^- = HgCl_3^-$	14.93	Powell et al. (2005)
8	$Hg^{2+} + 4Cl^- = HgCl_4^{2-}$	15.5	Powell et al. (2005)
9	$Hg^{2+} + SO_4^{2-} = HgSO_4$	2.6	Powell et al. (2005)
10	$Hg^{2+} + CO_3^{2-} = HgCO_3$	11.51	Powell et al. (2005)
11	$Hg^{2+} + 2CO_3^{2-} = Hg(CO_3)_2^{2-}$	15.58	Martell et al. (2001)
12	$Hg^{2+} + OH^- + CO_3^{2-} = Hg(OH)CO_3^-$	19.34	Powell et al. (2005)
13	$Hg^{2+} + H^+ + CO_3^{2-} = HgHCO_3^+$	15.84	Powell et al. (2005)
14	$Hg^{2+} + HS^- = HgSH^+$	22.3	Jay et al. (2000)
15	$Hg^{2+} + 2HS^- = Hg(SH)_2$	40.37	Jay et al. (2000)
16	$Hg^{2+} + 2HS^- + OH^- = HgS_2H^- + H_2O$	48.6	Jay et al. (2000)
17	$Hg^{2+} + 2HS^- + 2OH^- = HgS_2^{2-} + 2H_2O$	53.56	Jay et al. (2000)
18	$Hg^{2+} + HS^- + OH^- = HgS_{aq} + H_2O$	43.8	Jay et al. (2000)
19	$Hg^{2+} + HS^- + 2OH^- + 4S(0) = HgS_5OH^- + H_2O$	77.85	Jay et al. (2000)
20	$Hg^{2+} + 2HS^- + 2OH^- + 8S(0) = Hg(S_5)_2^{2-} + 2H_2O$	108.3	Jay et al. (2000)
21	$Hg^{2+} + R_{HA}{}^z = R_{HA}Hg^{z+2}$	3.6	Tipping (2007)
22	$Hg^{2+} + R_{FA}{}^z = R_{FA}Hg^{z+2}$	3.1	Tipping (2007)
23	$HgS_{(s,\ cinnabar)} + H^+ = HS^- + Hg^{2+}$	-39.1	Martell et al. (2003)
24	$HgO_{(s)} + H_2O = Hg^{2+} + 2OH^-$	-25.45	Martell et al. (2003)
25	$MeHg^+ + OH^- = MeHgOH$	9.47	De Robertis et al. (1998)
26	$2MeHg^+ + OH^- = (MeHg)_2OH^+$	11.85	De Robertis et al. (1998)
27	$MeHg^+ + CO_3^{2-} = MeHgCO_3^-$	6.1	Rabenstein et al. (1976)
28	$MeHg^+ + H^+ + CO_3^{2-} = MeHgHCO_3$	12.95	Loux (2007)
29	$MeHg^+ + Cl^- = MeHgCl$	5.45	De Robertis et al. (1998)
30	$MeHg^+ + SO_4^{2-} = MeHgSO_4^-$	2.64	De Robertis et al. (1998)
31	$MeHg^+ + HS^- = MeHgSH$	14.5	Loux (2007)
32	$MeHg^+ + HS^- + OH^- = MeHgS^- + H_2O$	21.0	Martell et al. (2001)
33	$2MeHg^+ + HS^- + OH^- = (MeHg)_2S + H_2O$	37.3	Martell et al. (2001)
34	$3MeHg^+ + HS^- + OH^- = (MeHg)_3S^+ + H_2O$	44.3	Martell et al. (2001)
35	$MeHg^+ + R_{HA}{}^z = R_{HA}MeHg^{z+1}$	0.3	Tipping (2007)
36	$MeHg^+ + R_{FA}{}^z = R_{FA}MeHg^{z+1}$	0.3	Tipping (2007)
37	$FeS_{(s,\ mackinawite)} + H^+ = Fe^{2+} + HS^-$	-3.5	Rickard (2006)

[a]: $R_{HA}{}^z$ and $R_{FA}{}^z$ represent humic and fulvic acid molecules, respectively.

Table 3. Concentrations of C_{org}, Fe-ox, Hg_T and MeHg in the top 0.5-cm layer of Lake Tantaré Basin A sediments as well as molar ratios in this sediment layer and in the Fe-rich material collected with the Teflon sheets.

	Lake Tantaré Basin A	
	Top sediment layer	Teflon sheets
Concentration		
{C_{org}} mol C g^{-1}	$2.02 \pm 0.08 \times 10^{-2}$	
{Fe-ox} mol g^{-1}	$1.55 \pm 0.05 \times 10^{-3}$	
{Hg_T} mol g^{-1}	$3.0 \pm 0.1 \times 10^{-9}$	
{MeHg} mol g^{-1}	$7.6 \pm 1.1 \times 10^{-11}$	
Molar ratio		
{C_{org}}:{Fe-ox}	13	2.6 ± 0.3
{C_{org}}:{N}	15.5	15.3 ± 3.4
{Hg_T}:{Fe-ox}	1.9×10^{-6}	$1.3 \pm 0.3 \times 10^{-7}$
{MeHg}:{Fe-ox}	4.9×10^{-8}	$6.5 \pm 1.9 \times 10^{-10}$
{Hg_T}:{C_{org}}	1.5×10^{-7}	$4.9 \pm 0.7 \times 10^{-8}$
{MeHg}:{C_{org}}	3.8×10^{-9}	$2.5 \pm 0.6 \times 10^{-10}$

Table 4. R_{net}^{Hg} as a function of depth calculated with the computer code PROFILE for each of the two study basins of Lake Tantaré and sampling date along with estimated present-day fluxes of Hg due to particle settling (J_{Dep}^{Hg}) and to the transport of dissolved Hg across the sediment−water interface by molecular diffusion (J_{D}^{Hg}), bioirrigation (J_{I}^{Hg}), and biodiffusion (J_{B}^{Hg}), and net Hg accumulation fluxes (J_{Acc}^{Hg}).

Sampling Date	Zone No.	Depth interval cm	R_{net}^{Hg}	J_{Dep}^{Hg}	J_{D}^{Hg}	J_{I}^{Hg}	J_{B}^{Hg}	J_{Acc}^{Hg}
			10^{-21} mol cm^{-3} s^{-1}	10^{-21} mol cm^{-2} s^{-1}				
Basin A								
Sept. 05	1	0-6.3	-0.7	544	0.95	0.27	4.3×10^{-4}	545
	2	6.33-9.5	2.4					
Sept. 06	1	0-9.5	-0.8	544	0.24	0.058	1.1×10^{-4}	544
Basin B								
Oct. 06	1	0-4.1	-14	765	65.8	0	0	821
	2	4.1-9.5	1.7					
July 07	1	0-5.7	-3.6	765	18.6	0	0	784
	2	5.7-8.5	11					

Table 5. R_{net}^{MeHg} as a function of depth calculated with the computer code PROFILE for each of the two study basins of Lake Tantaré and sampling date along with estimated present-day fluxes of MeHg due to particle settling (J_{Dep}^{MeHg}) and to the transport of dissolved MeHg across the sediment−water interface by molecular diffusion (J_{D}^{MeHg}), bioirrigation (J_{I}^{MeHg}), and biodiffusion (J_{B}^{MeHg}), and net MeHg accumulation fluxes (J_{Acc}^{MeHg}). To estimate J_{Dep}^{MeHg}, we assumed that the production or degradation of MeHg in surface sediments is negligible.

Sampling Date	Zone No.	Depth interval cm	R_{net}^{MeHg} 10^{-21} mol cm^{-3} s^{-1}	J_{Dep}^{MeHg}	J_{D}^{MeHg}	J_{I}^{MeHg}	J_{B}^{MeHg}	J_{Acc}^{MeHg}
				10^{-21} mol cm^{-2} s^{-1}				
Basin A								
Sept. 05	1	0-4.7	-0.2	14.1	0.20	0.020	0.7×10^{-4}	14.3
	2	4.7-9.5	0.3					
Sept.06	1	0-1.2	-1.1	14.1	-0.39	-0.099	-1.4×10^{-4}	13.6
	2	1.2-2.4	2.1					
	3	2.4-5.9	-0.3					
	4	5.9-9.5	0.1					
Basin B								
Oct. 06	1	0-1.6	-3.5	4.65	5.70	0	0	10.3
	2	1.6-9.5	-0.01					
July 07	1	0-3.2	-0.9	4.65	4.05	0	0	8.7
	2	3.2-9.5	-0.03					

CAPTIONS FOR FIGURES

Figure 1. Location map of Lakes Tantaré, Bédard and Holland. Inset: Lake Tantaré and its watershed, including the sampling location in Basins A and B.

Figure 2. Triplicate porewater profiles of Hg_T (a-d), MeHg (e-h), Fe and Mn (i-l), ΣS(-II) (m-p), ΣS(0) (q-t), and SO_4 (u-x) concentrations for Basin A of Lake Tantaré in September 2005 and in September 2006 and for Basin B of Lake Tantaré in October 2006 (anoxic period) and in July 2007 (oxic period). The circle, triangle and square symbols are for triplicate water samples for either the measurements of Hg_T, MeHg, Fe and Mn or those of ∑S(-II), ∑S(0), and SO_4. Empty symbols in panels a-h and m-t represent concentrations below detection limit. The horizontal dotted lines indicate the sediment−water interface.

Figure 3. Depth profiles of the main species of dissolved Hg_{NM} (a-d) and of dissolved MeHg (e-h) for Lake Tantaré Basins A and B. The percentages of the dissolved species of inorganic Hg and MeHg were calculated with the speciation model WHAM 6. Comparison of modeled and measured average (n=3) concentration of dissolved Hg_T (i-l) and MeHg (m-p) with the horizontal dotted lines indicating the sediment−water interface, the piecewise constant functions (thick solid lines) representing the net Hg_T and MeHg production (+) /consumption (-) rate (R_{net}^{Hg} and R_{net}^{MeHg}) and the thin solid lines following the measured values showing the PROFILE model fitting. Saturation index (SI = log (IAP/K_s) profiles for $FeS_{(s,\ m)}$ (disordered mackinawite; K_s = -3.5) is also given (q-t).

Figure 4. Depth profiles of {Hg_T} and {Hg_T}:{Al} molar ratio (a-d), {MeHg} (e-f), {Fe} and {Mn} (g-j), {C_{org}} (k-n), and {S_T} and {AVS} (o-r) in Lake Tantaré Basins A and B and in Lakes Bédard and Holland.

Figure 5. Comparison of modeled and measured concentration of dissolved MeHg (a-c) for Basin A in September 2006 with the horizontal dotted lines indicating the sediment−water interface, the piecewise constant functions (thick solid lines) representing the net MeHg production (+) /consumption (-) rate (R_{net}^{MeHg}) and the thin solid lines following the measured values showing the PROFILE model fitting.

Figure 6. Reconstructed historical records of anthropogenic Hg deposition fluxes to the sediments of Lake Tantaré (a) Basins A (filled circles) and B (open circles), of Lake Bédard (b) and of Lake Holland (c) corrected for lake specific processes ($J_{Corr}^{Hg-Anth}$); the insets show the records uncorrected for such processes ($J^{Hg-Anth}$).

FIGURES – Feyte et al.

Mercury dynamics in lake sediments

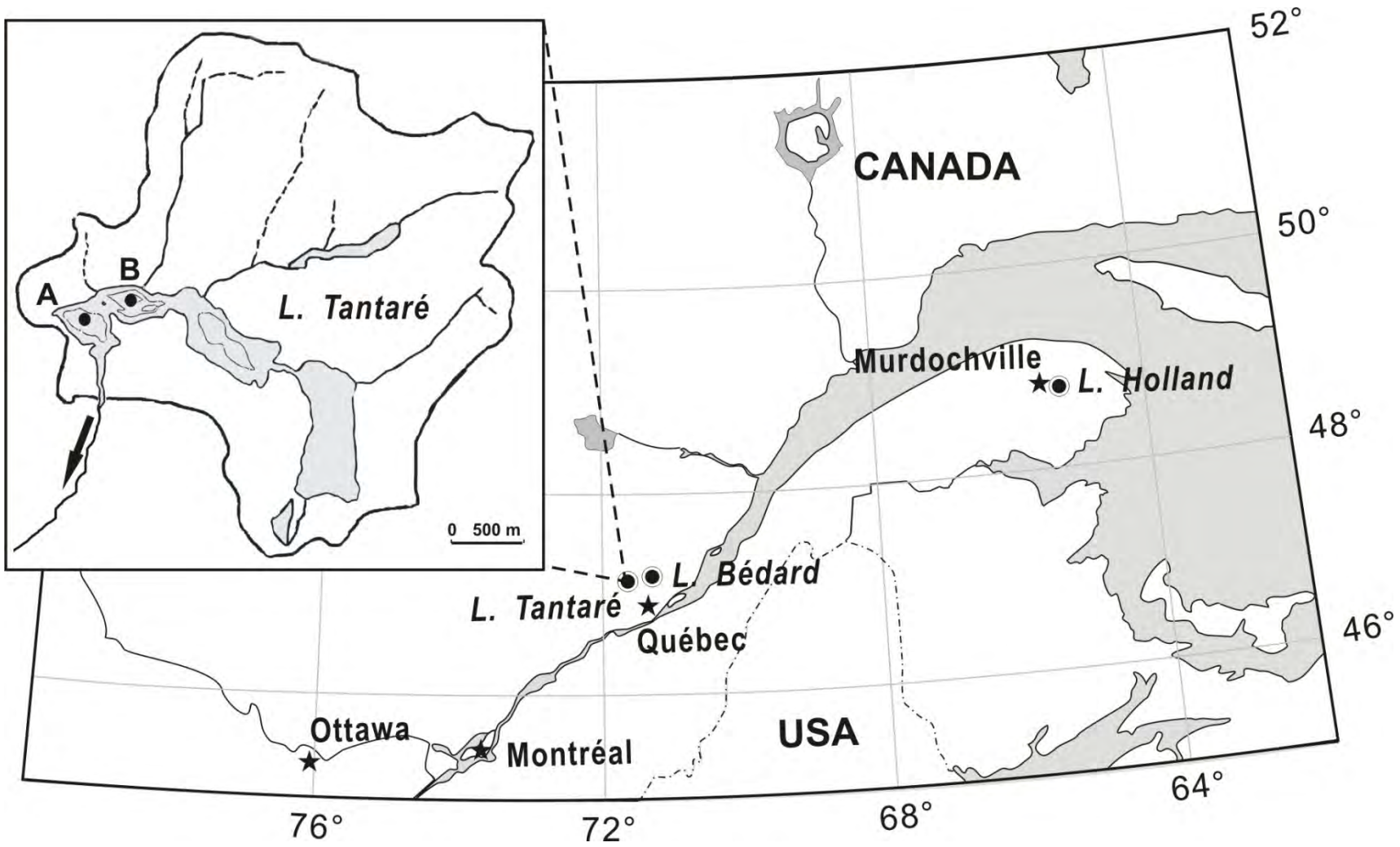
A
B
L. Tantaré
0 500 m
CANADA
USA
Murdochville
L. Holland
L. Bédard
L. Tantaré
Québec
Ottawa
Montréal
52°
50°
48°
46°
76°
72°
68°
64°

Fig. 1

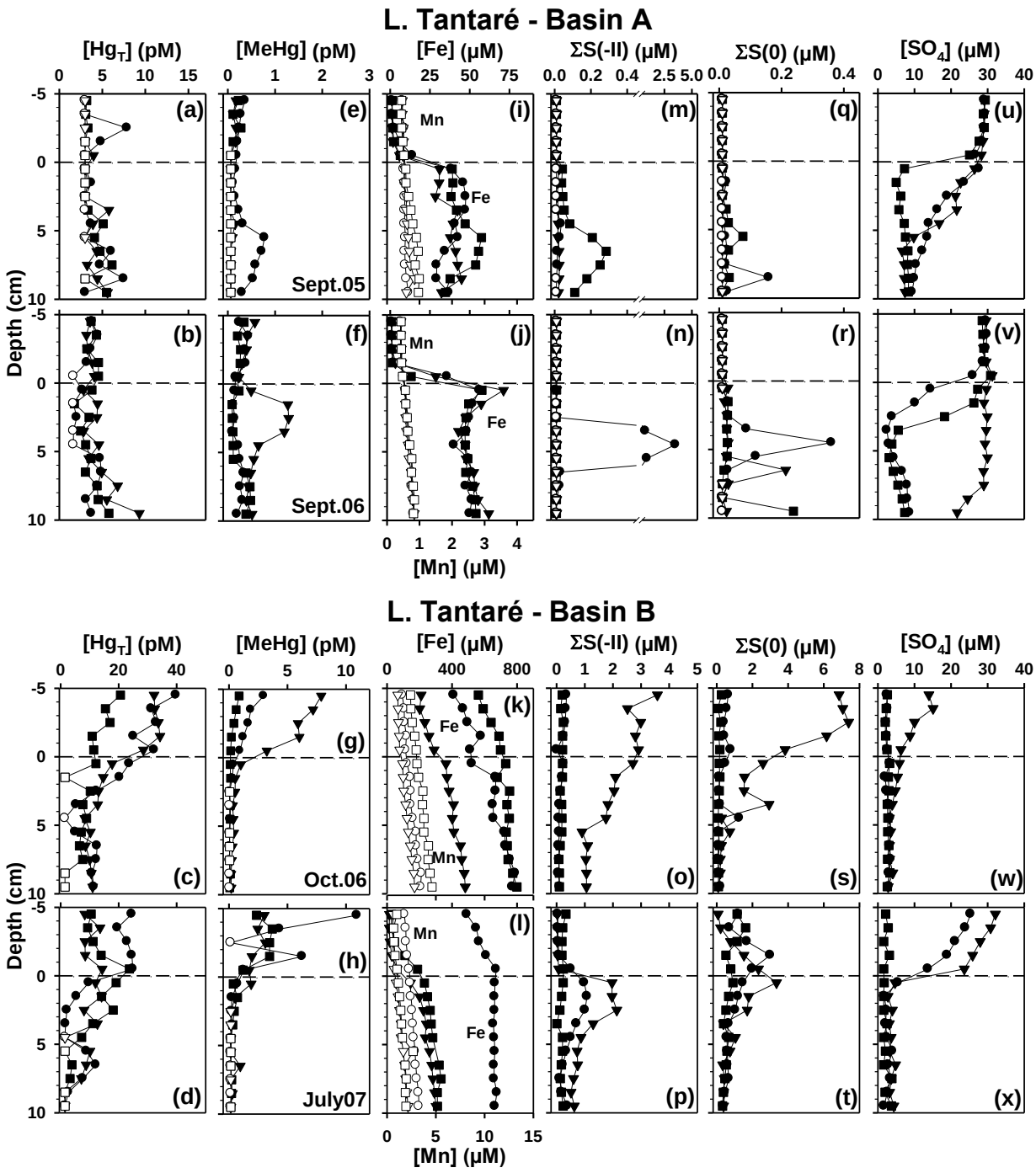
L. Tantaré - Basin A
[Hg$_T$] (pM)
[MeHg] (pM)
[Fe] (μM)
ΣS(-II) (μM)
ΣS(0) (μM)
[SO$_4$] (μM)
Depth (cm)
(a)
(e)
(i)
(m)
(q)
(u)
(b)
(f)
(j)
(n)
(r)
(v)
Mn
Fe
Sept.05
Sept.06
[Mn] (μM)
L. Tantaré - Basin B
(c)
(g)
(k)
(o)
(s)
(w)
(d)
(h)
(l)
(p)
(t)
(x)
Oct.06
July07

Fig. 2

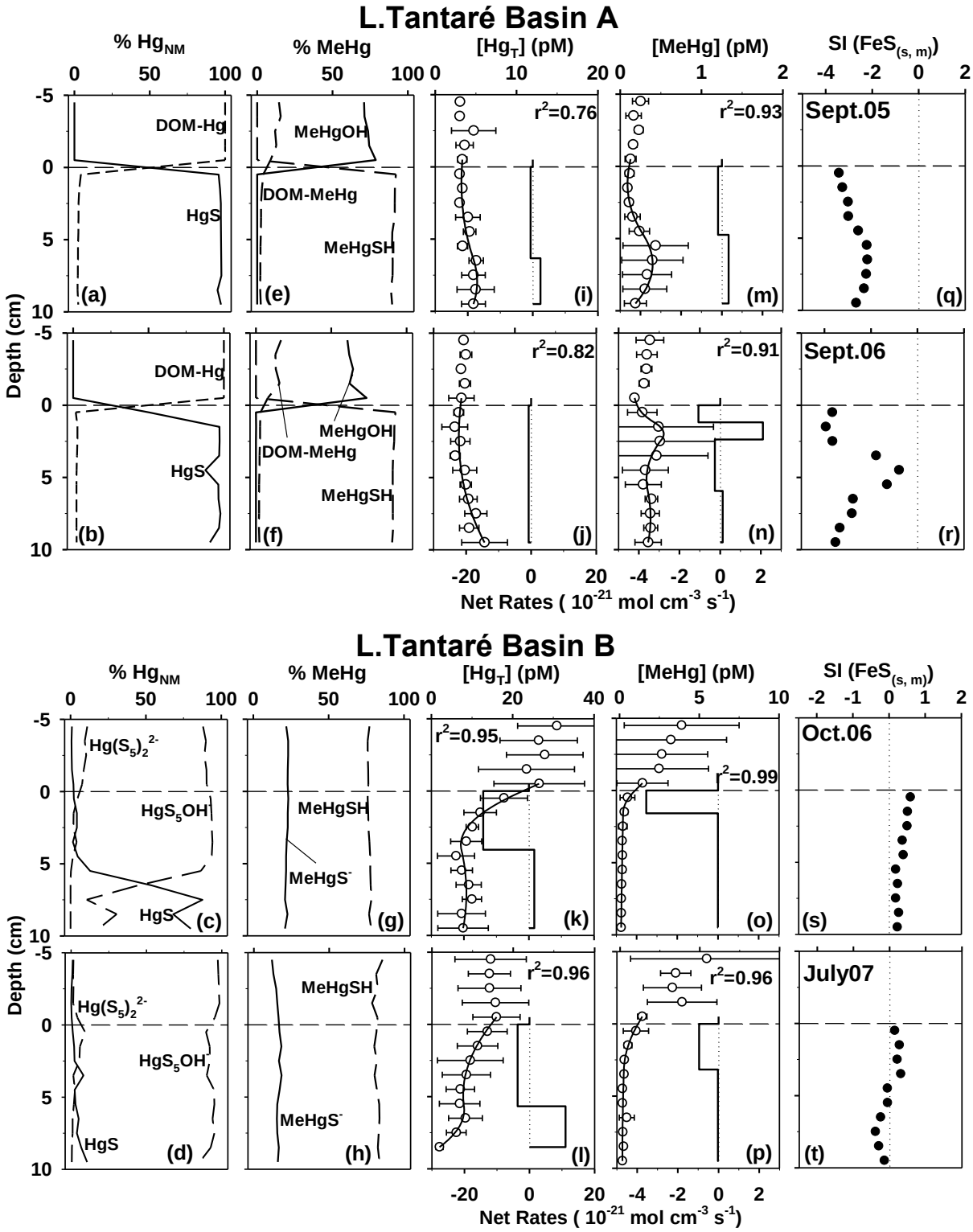
L.Tantaré Basin A
% Hg_NM
% MeHg
[Hg_T] (pM)
[MeHg] (pM)
SI (FeS_(s, m))
DOM-Hg
HgS
MeHgOH
DOM-MeHg
MeHgSH
r²=0.76
r²=0.93
r²=0.82
r²=0.91
Sept.05
Sept.06
(a)
(b)
(e)
(f)
(i)
(j)
(m)
(n)
(q)
(r)
Depth (cm)
Net Rates (10^-21 mol cm^-3 s^-1)
L.Tantaré Basin B
Hg(S5)2 2-
HgS5OH
HgS
MeHgSH
MeHgS-
r²=0.95
r²=0.99
r²=0.96
Oct.06
July07
(c)
(d)
(g)
(h)
(k)
(l)
(o)
(p)
(s)
(t)

Fig. 3

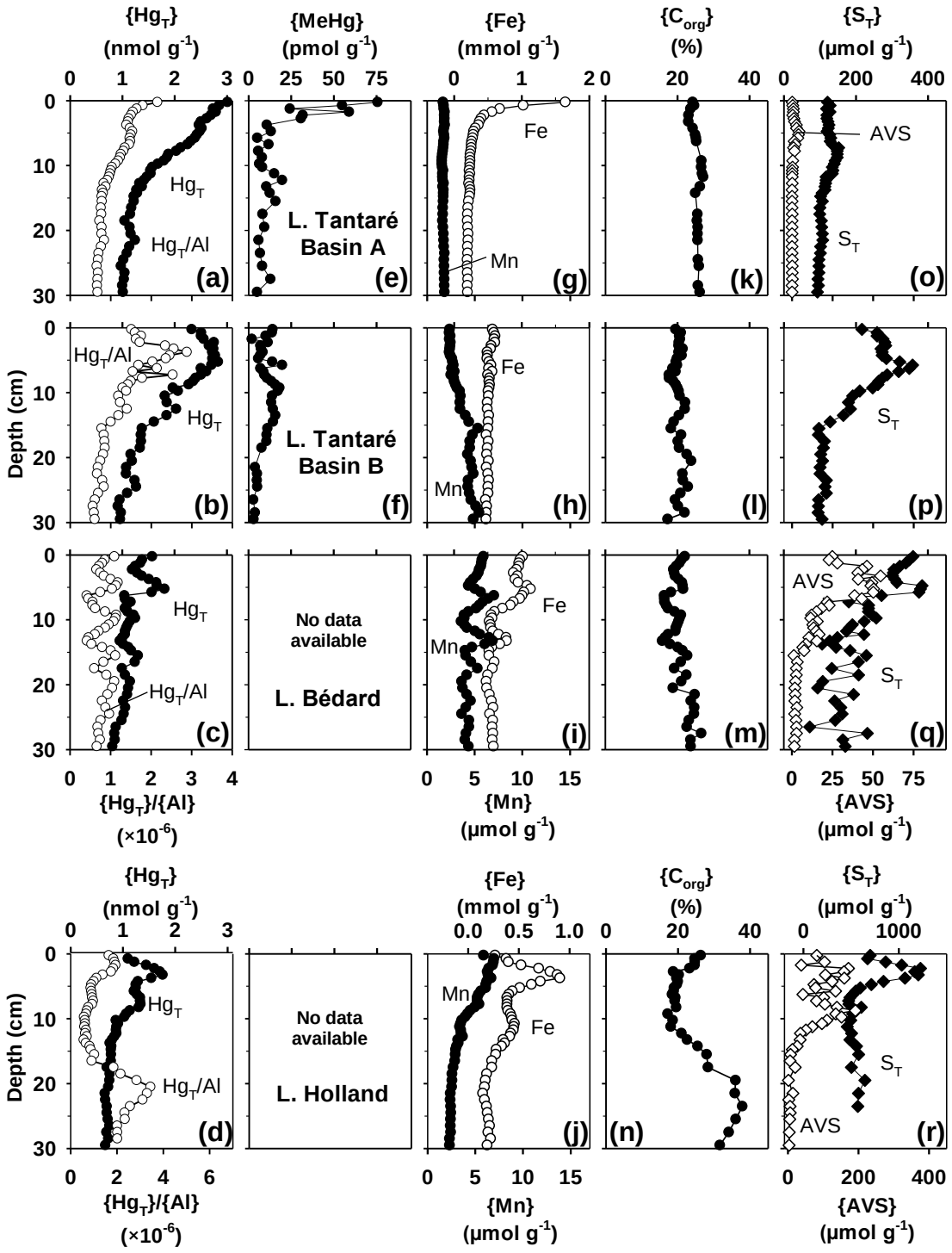
{Hg_T} (nmol g^-1)
{MeHg} (pmol g^-1)
{Fe} (mmol g^-1)
{C_org} (%)
{S_T} (µmol g^-1)
Hg_T
Hg_T/Al
Fe
Mn
AVS
S_T
L. Tantaré Basin A
L. Tantaré Basin B
L. Bédard
L. Holland
No data available
Depth (cm)
{Hg_T}/{Al} (×10^-6)
{Mn} (µmol g^-1)
{AVS} (µmol g^-1)
(a)
(b)
(c)
(d)
(e)
(f)
(g)
(h)
(i)
(j)
(k)
(l)
(m)
(n)
(o)
(p)
(q)
(r)

Fig. 4

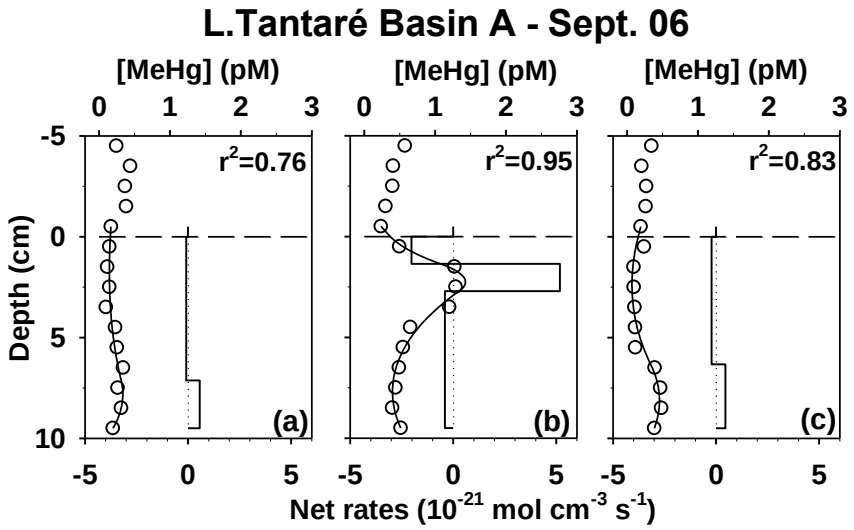
L.Tantaré Basin A - Sept. 06
[MeHg] (pM)
[MeHg] (pM)
[MeHg] (pM)
0 1 2 3
0 1 2 3
0 1 2 3
-5
0
5
10
Depth (cm)
r2=0.76
r2=0.95
r2=0.83
(a)
(b)
(c)
-5 0 5
-5 0 5
-5 0 5
Net rates (10-21 mol cm-3 s-1)

Fig. 5

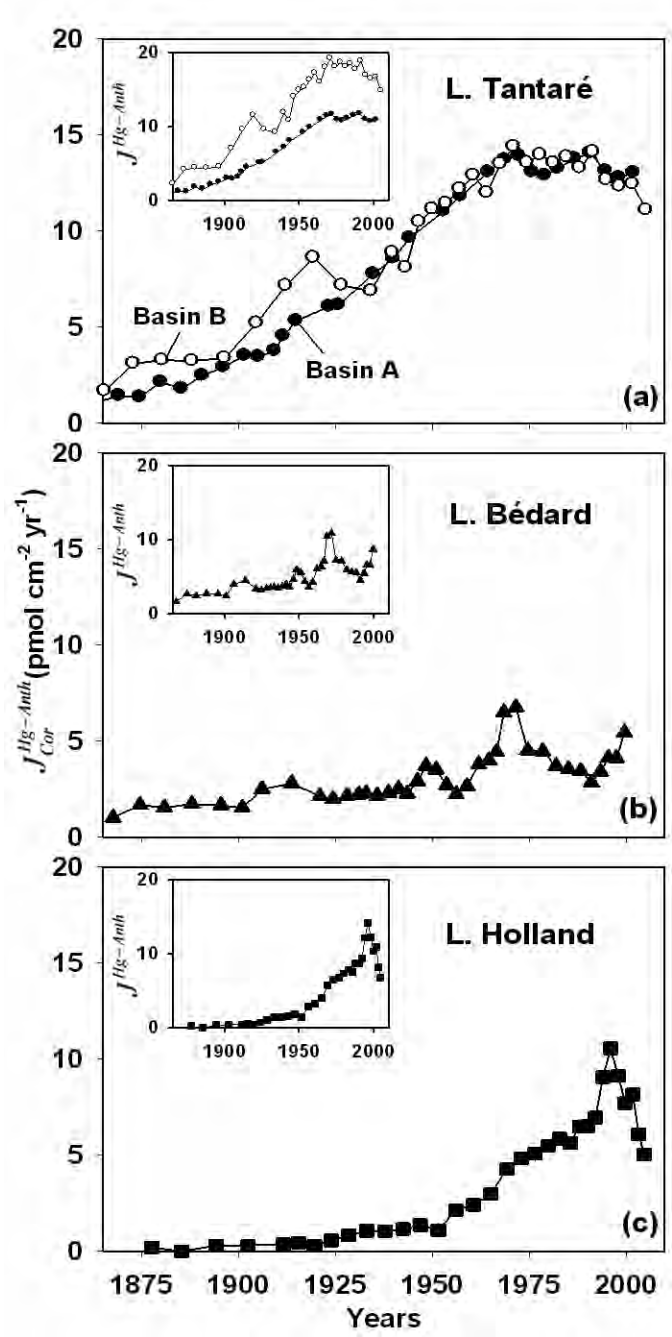
L. Tantaré
Basin B
Basin A
(a)
L. Bédard
(b)
L. Holland
(c)
$J^{Hg-Anth}_{Cor}$ (pmol cm^{-2} yr^{-1})
$J^{Hg-Anth}$
Years
1875
1900
1925
1950
1975
2000

Fig. 6